Master's Thesis

Effect of Chirality on Poly(azidohexyl glycidyl ether)s

Yungyeong Lee

Department of Chemistry

Graduate School of UNIST

2019

Effect of Chirality on Poly(azidohexyl glycidyl ether)s

Yungyeong Lee

Department of Chemistry

Graduate School of UNIST

Effect of Chirality on Poly(azidohexyl glycidyl ether)s

A thesis/dissertation
submitted to the Graduate School of UNIST
in partial fulfillment of the
requirements for the degree of
Master of Science

Yungyeong Lee

12/14/2018 of submission
Approved by

_____

Advisor
Tae-Hyuk Kwon

Effect of Chirality on Poly(azidohexyl glycidyl ether)s

Yungyeong Lee

This certifies that the thesis/dissertation of Yungyeong Lee is approved.

12/14/2018 of submission

signature

_____

Advisor: Tae-Hyuk Kwon

signature

_____

Byeong-Su Kim: Thesis Committee Member #1

signature

_____

Dong Woog Lee: Thesis Committee Member #2;

Abstract

Poly(ethylene glycol) (PEG) is one of the most widely used synthetic biocompatible polymers; however, its limited functionality often poses significant challenges for advanced applications. The functionality can be incorporated by directly introducing functional groups along the polymer backbone or by post-polymerization modification. On the other hand, chirality which is one of the most intriguing concepts has been proven to govern numerous key biological processes. Despite the importance, effects of chirality or tacticity on polyethers and their applications have been rarely reported.

Therefore, this thesis aims to study the effect of chirality on poly(azidohexyl glycidyl ether)s (PAHGEs). We prepared the chiral azidohexyl glycidyl ether (AHGE) monomer to form isotactic polymers with opposite backbone chiralities. Although the polymers were not fully isotactic as confirmed by ^{13}C NMR, their enantiomeric mixtures were subjected to GPC and DSC measurements for further studies e.g. stereocomplexation. Lastly, the chiral hexyl glycidyl ether (HGE) monomer and the resulting polymers, poly(hexyl glycidyl ether)s (PHGEs) were prepared as well for comparative analysis on the effect of azide moieties. The effect of backbone chiralities were much more significant in crystallizable PHGEs than amorphous PAHGEs but neither of them formed stereocomplex.

Contents

List of Figures

List of Tables

Abbreviations

I. Introduction 1

1.1 Polyether 1

1.1.1 Poly(ethylene glycol) 1

1.1.2 Polyglycerol 1

1.1.3 Functionalized PG 1

1.2 Tacticity-controlled polyether 3

1.2.1 Tacticity 3

1.2.2 Tacticity-controlled polyether 3

1.2.3 Methods to confirm the tacticity 3

1.2.4 Synthesis and relevant studies 4

1.3 Stereocomplex 6

1.3.1 Definition 6

1.3.2 Methods to characterize stereocomplexation 7

1.3.3 Applications 7

II. Experimental section 11

2.1 Synthesis and characterization of isotactic PAHGEs 11

2.2 Investigation on stereocomplexation of the isotactic P(A)HGEs 13

III. Results and Discussion 16

3.1 Synthesis and characterization of isotactic PAHGEs 16

3.2 Investigation on stereocomplexation of the isotactic P(A)HGEs 23

IV. Conclusion 38

V. References 39

Acknowledgements

List of Figures

Figure 1. (a) Chemical structures of PEG and linear PG. (b) Available topological variety based on linear PG building blocks.

Figure 2. Synthetic scheme of isotactic polyethers.

Figure 3. Design scheme of bimetallic enantioselective catalyst for isotactic polyether synthesis.

Figure 4. Various methods used to characterize PMMA stereocomplex.

Figure 5. Stereocomplexation of poly(propylene succinate).

Figure 6. Synthetic scheme of (a) the (*S*)-AHGE monomer and (b) the (*S*)-PAHGE.

Figure 7. Representative (a) ^{1}H and (b) ^{13}C NMR spectrum of the 6-azido-1-hexanol.

Figure 8. Representative (a) ^{1}H and (b) ^{13}C NMR spectrum of the (*S*)-AHGE monomer.

Figure 9. Representative ^{1}H NMR spectra (a) of the (*S*)-AHGE monomer, (b) taken after the full monomer conversion, (c) taken after *t*-Bu-P_4 filtration and (d) of the final PAHGE (entry 1 in Table 1).

Figure 10. Representative (a) ^{1}H and (b) ^{13}C NMR spectrum of the (*S*)-$PAHGE_{33}$ (entry 1 in Table 1).

Figure 11. FT-IR spectra of the products in each step.

Figure 12. Representative expanded ^{13}C NMR spectra of (a) (*S*)-$PAHGE_{33}$ and (b) (*R*)-$PAHGE_{28}$ for tacticity analysis.

Figure 13. GPC traces of (a) (*S*)-PAHGEs and (b) (*R*)-PAHGEs (eluent: DMF, calibration: PMMA).

Figure 14. GPC traces of (a) (*S*)-$PAHGE_{33}$, (b) (*R*)-$PAHGE_{28}$ and (c) $M_{n.GPC}$ (left) and M_w/M_n (right) for their mixtures at varying fractions.

Figure 15. GPC traces of the block copolymer $PAHGE_{27}$ (entry 4 in Table 2) after the first polymerization (dash) and the second polymerization (solid).

Figure 16. GPC traces of (a) (*S*)-PAHGEs and (b) (*R*)-PAHGEs (eluent: DMF, calibration: PMMA).

Figure 17. $M_{n.GPC}$ (left) and M_w/M_n (right) measured in DMF for the mixtures of (a) (*S*)-$PAHGE_{31}$/(*R*)-$PAHGE_{25}$, (b) (*S*)-$PAHGE_{49}$/(*R*)-$PAHGE_{49}$ and (c) (*S*)-$PAHGE_{100}$/(*R*)-$PAHGE_{98}$ at varying fractions.

Figure 18. GPC traces of (a) (*S*)-PAHGEs and (b) (*R*)-PAHGEs (eluent: $CHCl_3$, calibration: PMMA).

Figure 19. $M_{n.GPC}$ (left) and M_w/M_n (right) measured in $CHCl_3$ for the mixtures of (a) (*S*)-$PAHGE_{31}$/(*R*)-$PAHGE_{25}$, (b) (*S*)-$PAHGE_{49}$/(*R*)-$PAHGE_{49}$ and (c) (*S*)-$PAHGE_{100}$/(*R*)-$PAHGE_{98}$ at varying fractions.

Figure 20. DSC thermograms of (a) (*rac.*)-$PAHGE_{35}$, (b) (*S*)-$PAHGE_{31}$, (c) (*R*)-$PAHGE_{25}$ and (d) 1:1 blend of (*S*)-$PAHGE_{31}$ and (*R*)-$PAHGE_{25}$.

Figure 21. DSC thermograms of (a) (*S*)-$PAHGE_{49}$, (b) (*R*)-$PAHGE_{49}$, (c) 1:1 blend of (*S*)-$PAHGE_{49}$ and (*R*)-$PAHGE_{49}$, (d) (*S*)-$PAHGE_{100}$, (e) (*R*)-$PAHGE_{98}$ and (f) 1:1 blend of (*S*)-$PAHGE_{100}$ and (*R*)-$PAHGE_{98}$.

Figure 22. Synthetic scheme of (a) the (*S*)-HGE monomer and (b) the (*S*)-PHGE.

Figure 23. Representative (a) ^1H and (b) ^{13}C NMR spectrum of the (*S*)-HGE monomer.

Figure 24. Representative (a) ^1H and (b) ^{13}C NMR spectrum of the (*S*)-$PHGE_{37}$ (entry 2 in Table 4).

Figure 25. Expanded ^{13}C NMR spectra of PHGEs for tacticity analysis.

Figure 26. GPC traces of (a) (*rac.*)-$PHGE_{40}$, (b) (*S*)-$PHGE_{37}$ and (c) (*R*)-$PHGE_{42}$ (eluent: THF, calibration: PS).

Figure 27. DSC thermograms of (a) (*rac.*)-$PHGE_{40}$, (b) (*S*)-$PHGE_{37}$, (c) (*R*)-$PHGE_{42}$ and (d) 1:1 blend of (*S*)-$PHGE_{37}$ and (*R*)-$PHGE_{42}$.

Figure 28. Photographs of (a) (*rac.*)-$PHGE_{40}$, (b) (*S*)-$PHGE_{37}$ and (c) (*R*)-$PHGE_{42}$.

List of Tables

Table 1. Characterization data for PAHGEs.

Table 2. Characterization data for PAHGEs.

Table 3. Characterization data for PAHGEs.

Table 4. Characterization data for PHGEs.

Table 5. Phase transition behaviors for PHGEs.

Abbreviations

AHGE – azidohexyl glycidyl ether

(A)ROP – (anionic) ring opening polymerization

$CHCl_3$ – chloroform

DMF – *N*,*N*-dimethylformamide

DP – degree of polymerization

DSC – differential scanning calorimetry

ee – enantiomeric excess

EO – ethylene oxide

ESI-MS – electrospray ionization mass spectrometry

GPC – gel permeation chromatography

HGE – hexyl glycidyl ether

$M_{n.NMR}$ / $M_{n.GPC}$ – number average molecular weight determined by NMR / GPC

M_w – weight average molecular weight

M_w/M_n – dispersity

m/z – mass-to-charge ratio

NMR – nuclear magnetic resonance

PAHGE – poly(azidohexyl glycidyl ether)

PEG – poly(ethylene glycol)

PG – poly(glycidol)

PHGE – poly(hexyl glycidyl ether)

PMMA – poly(methyl methacrylate)

PO – propylene oxide

PP – polypropylene

PPO – poly(propylene oxide)

PS – polystyrene

ref. – reference

T_c – crystallization temperature

THF – tetrahydrofuran

T_g – glass transition temperature

T_m – melting temperature

XRD – x-ray diffraction

ΔH_c – crystallization enthalpy

ΔH_m – melting enthalpy

I. Introduction

1.1 Polyether

1.1.1 Poly(ethylene glycol)

Polyethers is a group of polymers with multiple ether functional groups. The simplest form is poly(ethylene oxide), PEO or poly(ethylene glycol), PEG. PEG possesses biocompatibility and superior solubility both in water and organic solvents, so has been widely used in various fields such as detergents, cosmetics and biomedical or pharmaceutical applications.[1,2] In particular, U.S. Food and Drug Administration (FDA) approved its usage for pharmaceutics which is called as PEGylation. PEGylation is to graft PEG on proteins or drugs. The resulting molecules had an increased hydrodynamic size to increase the circulation time thus therapeutic efficiency by reducing an elimination from kidney or blood stream.[3] However, it has to be noted that the potential cytotoxicity of PEG with different molecular weights have been controversially discussed as well.[4] Meanwhile, PEG has only two hydroxyl groups which can be post-modified at the both ends to limit the functionality. Ethylene oxide (EO), the monomer from which it is synthesized by ring opening polymerization (ROP), is toxic and gaseous to hamper easy synthesis.

1.1.2 Polyglycerol

If multiple hydroxyl groups are added on each side chain, the problem would be solved. This alternative is polyglycerol or polyglycidol (PG). The glycidol monomer becomes liquid to enable the facile synthesis by cationic or anionic ROP. The resulting multiple hydroxyl groups pave the way for diverse functionalities through conjugation of other molecules. While the advantages of PEG from the structural similarities were maintained. Therefore, PGs with various architectures or compositions have been synthesized and utilized in various applications so far (Figure 1).

1.1.3 Functionalized PG

One of the strategies is to design the glycidol-derived monomer with desired properties. For instance, our group designed glycidol monomer with a disulfide linkage to report the novel redox-degradable hyperbranched PGs.[5] Tetrahydropyranyl glycidyl ether (TGE) monomer was newly designed as a cyclic analogue of the well-known protected glycidol monomer, ethoxyethyl glycidyl ether (EEGE). The small modification to add a methylene linkage to form a 6-membered ring increased hydrophobicity to enhance stability of the micelles prepared from the block copolymer of PEG and PTGE while maintaining the property to be degraded at low pH.[6] Besides, post-polymerization modifications on well-defined PGs can widen the applications. For example, polymers

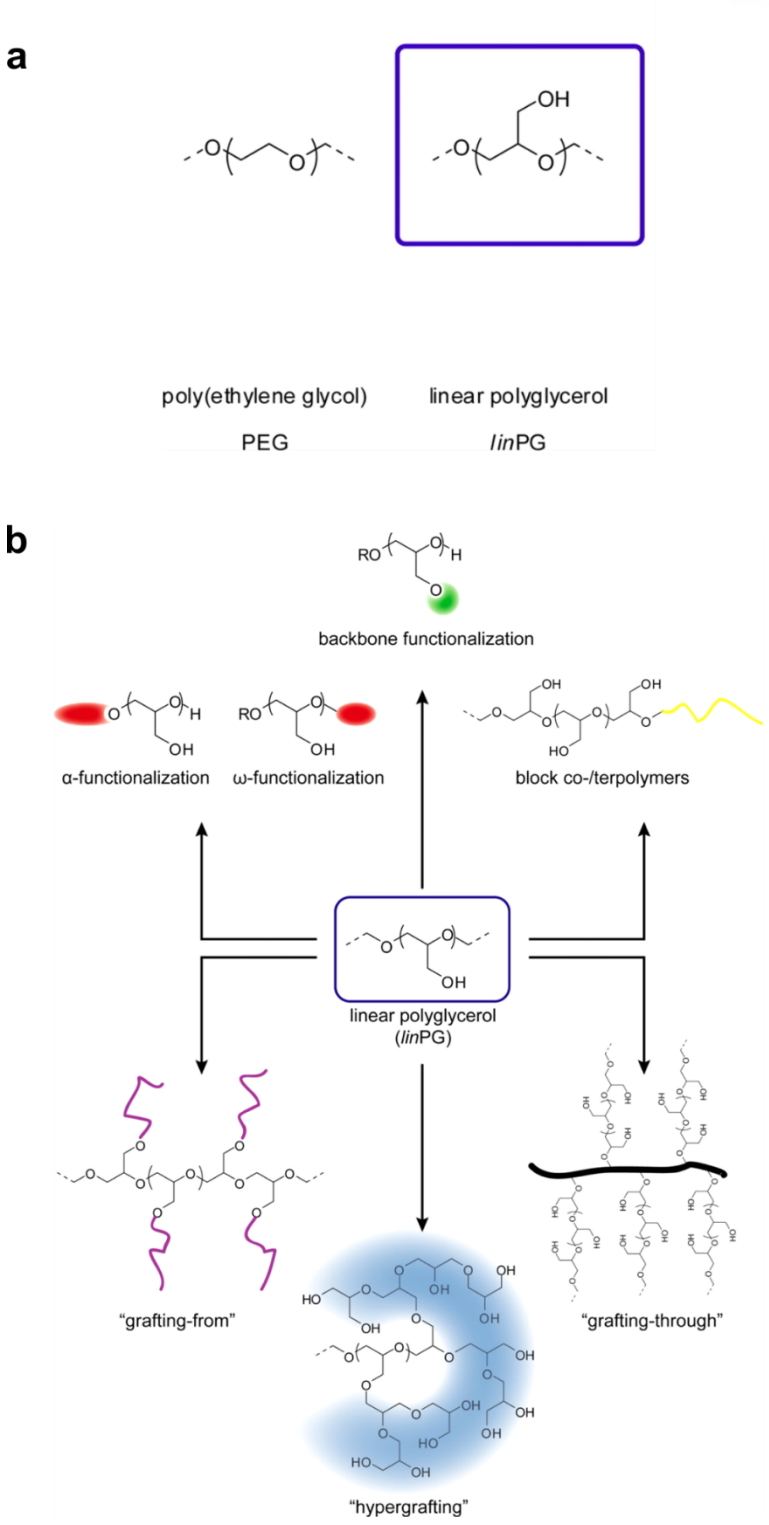

Figure 1. (a) Chemical structures of PEG and linear PG. (b) Available topological variety based on linear PG building blocks. Reprinted with permission from ref. [2]. Copyright 2014 American Chemical Society.

generated from allyl glycidyl ether (AGE) monomer have alkene groups on each side chain, so thiol-ene chemistry can be applied to introduce various functionalities. When various amine pendant groups were introduced to the copolymer of EO and AGE, the cloud points were tuned over wide range of temperatures.[7] However, to the best of our knowledge, synthesis or application of tacticity-controlled linear PGs have been rarely explored despite the importance of chirality which governs the nature and of tacticity which affects the polymer properties.

1.2 Tacticity-controlled polyether

1.2.1 Tacticity

Tacticity is about the way how side chains are arranged on main chain of polymers. Three cases are possible: isotactic, syndiotactic and atactic. If all side chains are on the same side, the polymer is isotactic. If side chains are alternating on either left or right side, the polymer is syndiotactic. Atactic polymers have no special pattern.

Among them, isotactic polymers are important in industry because the regular arrangement of pendant groups would favor a close packing to form crystals with impressive physical properties. For example, isotactic polypropylene (PP) whose polymerization was actively investigated in the 1950s with the development of the Ziegler-Natta catalyst is semicrystaline polymers (melting temperature or T_m=165–170 °C) in contrast to the amorphous atactic PP.[8] In 1957 the large-scale production of isotactic PP began, and it is still one of the most important industrial polymers to make up the second largest proportion (21%) of nonfiber plastics. The first place was taken by polyethylene (36%) which is also the vinyl polymers.[9]

1.2.2. Tacticity-controlled polyether

Apart from the vinyl polymers or polyolefins, tacticity of polyethers can be controlled as well because an asymmetric methine carbon makes the glycidyl ether monomer chiral. Similar to PP, isotactic poly(propylene oxide) (PPO) is semicrystaline (T_m=67 °C) in contrast to the amorphous atactic counterpart. Although isotactic PPOs are not commercialized as much as isotactic PPs, developing a synthetic method to realize the stereoregular sequence and investigating properties of the resulting polymers are main research areas.

1.2.3 Methods to confirm the tacticity

Before introducing the synthetic methods and relevant studies, methods to confirm the tacticity – ^{13}C NMR, DSC or X-ray scattering techniques and so on – are briefly described. First, ^{13}C NMR is direct and primitive way.[10] Along with the different arrangements or stereosequences, resonances of carbons on main chain arise from steric interactions between the substituents. For example, the

methine peak is split into triplet and the region on which the peak laid can be divided into *mm*, *mr/rm* and *rr* region. *mm* is an isotactic triad made up of two meso diads *RRR* or *SSS*. *rr* is a syndiotactic triad comprises two racemo diads *RSR* or *SRS*. The rest four sequences, *RRS, RSS, SSR* and *SRR* conform to *mr/rm* triad. The ratio between areas of distinct regions gives the ratio between the content of each triad thus the quantitative information of tacticity. Racemic polymers yield a triplet peak with the ratio between the area of *mm*, *mr*/*rm* and *rr* region as 1:2:1 whereas isotactic polymers give an unsplit singlet peak.

If a given sample is (semi)crystalline, DSC or X-ray scattering techniques can be used because tacticity affects crystallinity or physical property like T_m. Those methods are rather indirect and restrictive though allowing to merely infer some degree of isotacticity from crystallinity if the atactic analogue is amorphous.

1.2.4 Synthesis and relevant studies

From now on, the examples were limited to isotactic polyethers. Both regioselectivity and stereoregularity affect tacticity in brief. Several methods can be categorized in to three ways as shown in Figure 2.[11] Epoxide monomer with single substituent has two carbons: symmetric methylene carbon and asymmetric methine carbon. Regioselectivity is about how selectively one carbon is attacked over the other carbon for ring opening during the polymerization. When the chiral methine carbon is attacked, namely methine attack happens, stereoinversion do arise to reduce the stereoregularity. Thus, as shown in (a), regioselective catalyst is required to obtain isotactic polyether from enantiopure epoxide. However, when the monomer itself is not enantiopure, the common polymerization yields atactic polymer without any preference between (*R*)- and (*S*)-monomers or the methine and methylene attack within a molecule during the process. In this case, enantioselective catalyst (in (b)) or isoselective catalyst (in (c)) play a role. With the enantioselective catalyst, only one chiral form of the racemates participate in the process and the other remains. Coates and coworkers have been interested in establishing enantioselective polymerization to prepare stereoregular polyethers by designing and synthesizing appropriate catalyst.[12] The reasonable mechanism is also deduced from the crystal structure of the catalyst. The fundamental concept is to confine the geometry during the polymerization (Figure 3). Lastly, the isoselective catalyst is the most ideal case still under development where each chiral monomer separately yields two enantiomeric isotactic polymers even from the mixtures. Nevertheless, the use of special catalysts described above, has limitations on reaction conditions e.g. at low temperature to raise the catalytic selectivity.

Conventional or i.e. non-stereospecific polymerization technique, of course, has been adapted to polymerize enantiopure monomers, but the result was rather unsuccessful. For instance, McGrath *et al.* prepared the block copolymers consist of isotactic PPO and PEO by 18-crown-6-assisted anionic ring

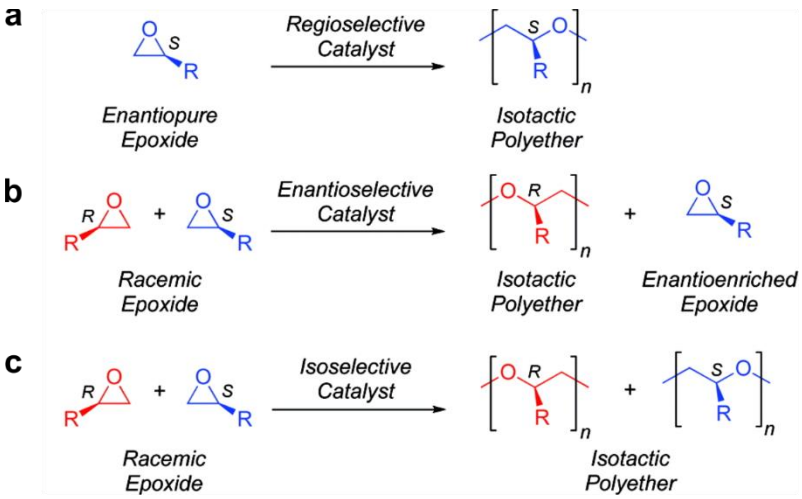

Figure 2. Synthetic scheme of isotactic polyethers. Reprinted with permission from ref. [11]. Copyright 2010 American Chemical Society.

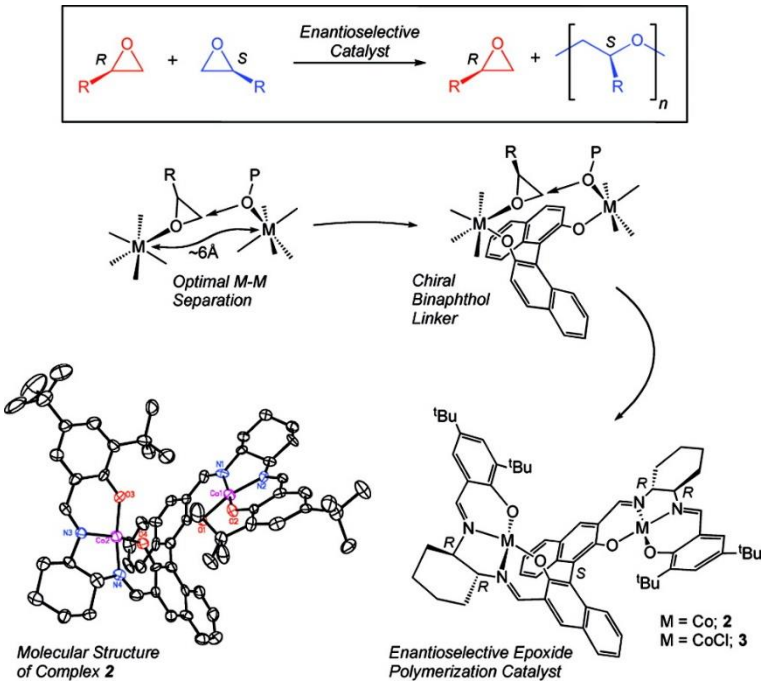

Figure 3. Design scheme of bimetallic enantioselective catalyst for isotactic polyether synthesis. Each metal center (M) coordinates the oxygen of the epoxide and alkoxide respectively. Mechanistic studies suggested that optimal M-M separation of ~6 Å offers an appropriate geometry for the enantioselective polymerization in case of cobalt. Reprinted with permission from ref. [12]. Copyright 2008 American Chemical Society.

opening polymerization (AROP) using potassium naphthalenide.[13] Enantiomeric (*R*)- and (*S*)-propylene oxide (PO) were prepared by hydrolytic kinetic resolution using (salen)Co^{III}-OAc complex. Once the racemic PO is dissolved in a solution of (*S*, *S*)-(salen)Co^{II} catalyst and glacial acetic acid, only (*R*)-PO reacts to give a diol product and unreacted (*S*)-PO remains. (*R*, *R*)-(salen)Co^{II} catalyst gives (*R*)-PO in the same way. Optical purity of kinetically resolved POs were determined by comparing the specific rotation value to the literature values. In spite of the extremely high optical purity of >99%, [*mm*] or content of isotactic *mm* triad of the isotactic polymers reached about 90%. The reason for not being fully isotactic was assumed as inevitable stereoinversion from small quantities of regioerrors.

However, the same AROP in which butanol worked as initiator and *t*-Bu-P_4 worked as base was successful as published by Satoh and coworkers.[14] *t*-Bu-P_4 (1-*tert*- butyl-4,4,4-tris(dimethylamino)-2,2-bis[tris(dimethylamino)-phosphoranylidenamino]-2Λ5,4Λ5-catenadi(phosphazene)) or simply phosphazene is an organic superbase synthesized by Schwesinger *et al.* and its effectiveness on ROP of EO has been shown.[15,16] Satoh's group has been shown that the system allows the successful synthesis of polyethers with various architectures and side groups 1) at mild condition (room temperature), 2) in living and controlled manner and 3) without chain transfer reaction.[14,17,18] In particular, in 2015, Isono *et al.* from the same research group reported for the first time that the system yielded isotactic polyethers when enantiopure (*S*)-*N,N*-dibenzylglycidylamine (DBGA) monomer was incorporated.[14] The mechanism behind was not covered thoroughly because the main objective of the paper was to introduce that the *t*-Bu-P_4/alcohol initiating system paved the way to controlled synthesis of polyethers with primary, secondary, and tertiary amino groups. After confirming the utility of the *t*-Bu-P_4/alcohol initiating AROP for the synthesis of isotactic polyethers, various epoxide monomers have been applied to study the effect of main chain tacticity on LCST behavior[19] or thin film formation.[20] In short, the impact on LCST behavior was negligible, but the latter study revealed that the isotacticity of side chains of brush block copolymers promoted better quality morphologies in terms of lateral ordering and orientation.

1.3 Stereocomplex

1.3.1 Definition

The efforts to develop routes to synthesize tacticity-controlled thus optically active polymers were expanded to the attention to how their binary blends would behave contrary to the components and eventually led to the discovery of stereocomplex, the unique phenomenon. The stereocomplex means basically a complex composed of complementing molecules.[21] DNA double helix made of two antiparallel complementary strands based on hydrogen bonding or collagen made of triple helices based mainly on coulombic interaction are some of notable examples in life. Strikingly, it was found

that even synthetic polymers can form so-called polymeric stereocomplex.

The first example was the pair between isotactic and syndiotactic poly(methyl methacrylate) (PMMA) found by Fox *et al.* in 1958.[22] The researchers synthesized isotactic, syndiotactic and their block copolymer-like PMMAs which had an ability to form crystals with varying melting properties and X-ray diffraction patterns. Based on the fact that the X-ray pattern of the last case was identical to that of mixtures of isotactic and syndiotactic PMMAs, Liquori *et al.* presumed later that there would exist a stereospecific interaction to form the new crystal.[23] Their comprehensive studies not only elucidated that the interaction occurred when the ratio between syndiotactic and isotactic PMMAs is near 2:1, but also proposed the model structure based on the assumption that Van der Waals interactions ascribed to the structural complementarity of two chains brought the formation of stereocomplex. The case was not limited to PMMA, so afterwards other examples including (*R*)- and (*S*)-poly(γ-benzylglutamate)[24] or poly($_L$-lactide) and poly($_D$-lactide)[25] and so on were reported.

1.3.2 Methods to characterize stereocomplexation

As stereocomplex is the formation of new crystallites, they can be characterized by a variety of spectroscopic and thermodynamic studies or imaging techniques. Some of them are illustrated in Figure 4 and 5. First, aggregation increases turbidity of polymeric solution, so the ratio between two polymers where turbidity distinctly increases tells the composition as Liquori *et al.* performed (Figure 4 (a)). Second, thermodynamic studies like differential scanning calorimetry (DSC) can be used to inspect the altered physical properties of the stereocomplex (Figure 4 (d) and Figure 5 (b)). Interlocked conformations increase crystallinity and melting temperatures. The T_m increase by approximately 50 °C was observed in the case of polylactide (PLA).[25] At last, the new crystalline structure gives different X-ray diffraction (XRD) profiles (Figure 4 (d) and Figure 5 (c)) and can be visualized further by atomic force microscopy (AFM) as well (Figure 4 (c)). Nowadays, the emergence of cutting-edge technologies and precision polymerization techniques enabled more precise investigations on such as structural details[26], how long is the critical chain length required or effects of molecular weight and dispersity on the PMMA stereocomplex formation.[27]

1.3.3 Applications

After their discoveries, stereocomplex has been applied widely. In detail, the formation of PMMA stereocomplex has been utilized to develop a solid-phase molecular-scale template to synthesize stereoregular PMMA.[28] The selective extraction of one polymer from the stereocomplex film rendered porous film made of the other polymer with structurally regulated nanospaces. The mechanism was proved as the slow incorporation of monomer followed by stepwise polymerization to fill the confined space. For example, the remained syndiotactic PMMA successfully resulted in complementary

isotactic PMMA with the high isotacticity of 92% and vice versa. Meanwhile, the complementary stereocomplexation of PLA drove hydrogelation.[29] Other applications of the stereocomplex of PLA or PLA-based copolymers are well introduced in reviews.[30,31] However, the most popular motivation is to achieve improved thermal and mechanical properties differ from parent polymers. Poly(propylene succinate)[32], a new class of polyesters which is not only biocompatible but also has a high T_m similar to low density polyethylene, or γ-butyrolactone-based polymer[33] are the recently reported examples. In each case, T_m was increased by around 40 °C and 80 °C compared to their enantiomers.

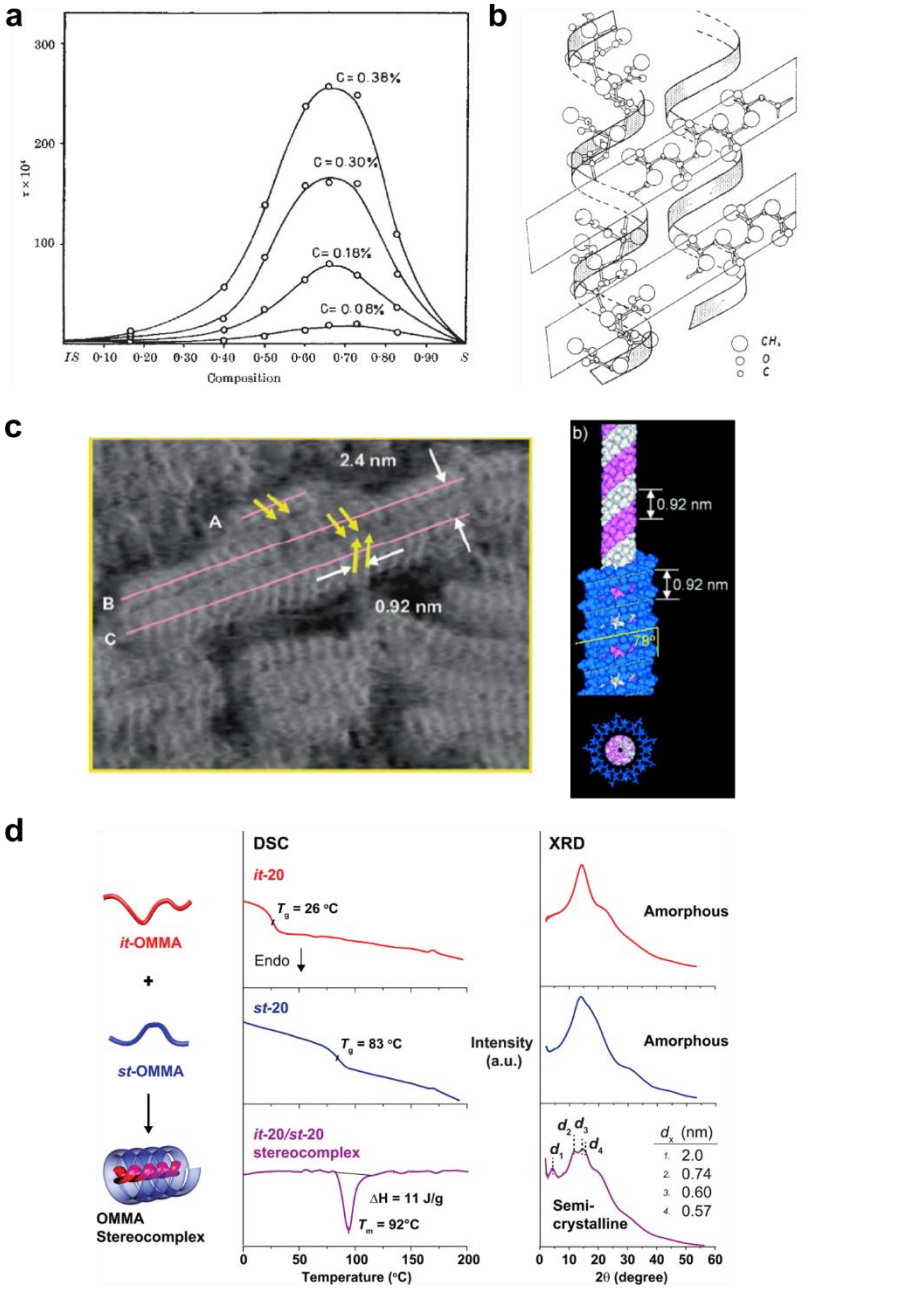

Figure 4. Various methods used to characterize PMMA stereocomplex. (a) Turbidity measurement of isotactic (*IS*)/syndiotactic (*S*) PMMA mixtures at varying composition and concentrations. (b) The first schematic structure of the stereocomplex presumed from XRD photograph. (c) Triple-stranded helix model (right; white and pink: isotactic-, blue: syndiotactic PMMA) elucidated by AFM image (left). (d) DSC thermograms and XRD patterns. Discrete oligomer synthesis allowed more precise investigation. Reprinted with permission from ref [23]. Copyright 1965 Springer Nature. Reprinted with permission from ref [26]. Copyright 2007 John Wiley and Sons. Reprinted with permission from ref. [27]. Copyright 2018 American Chemical Society.

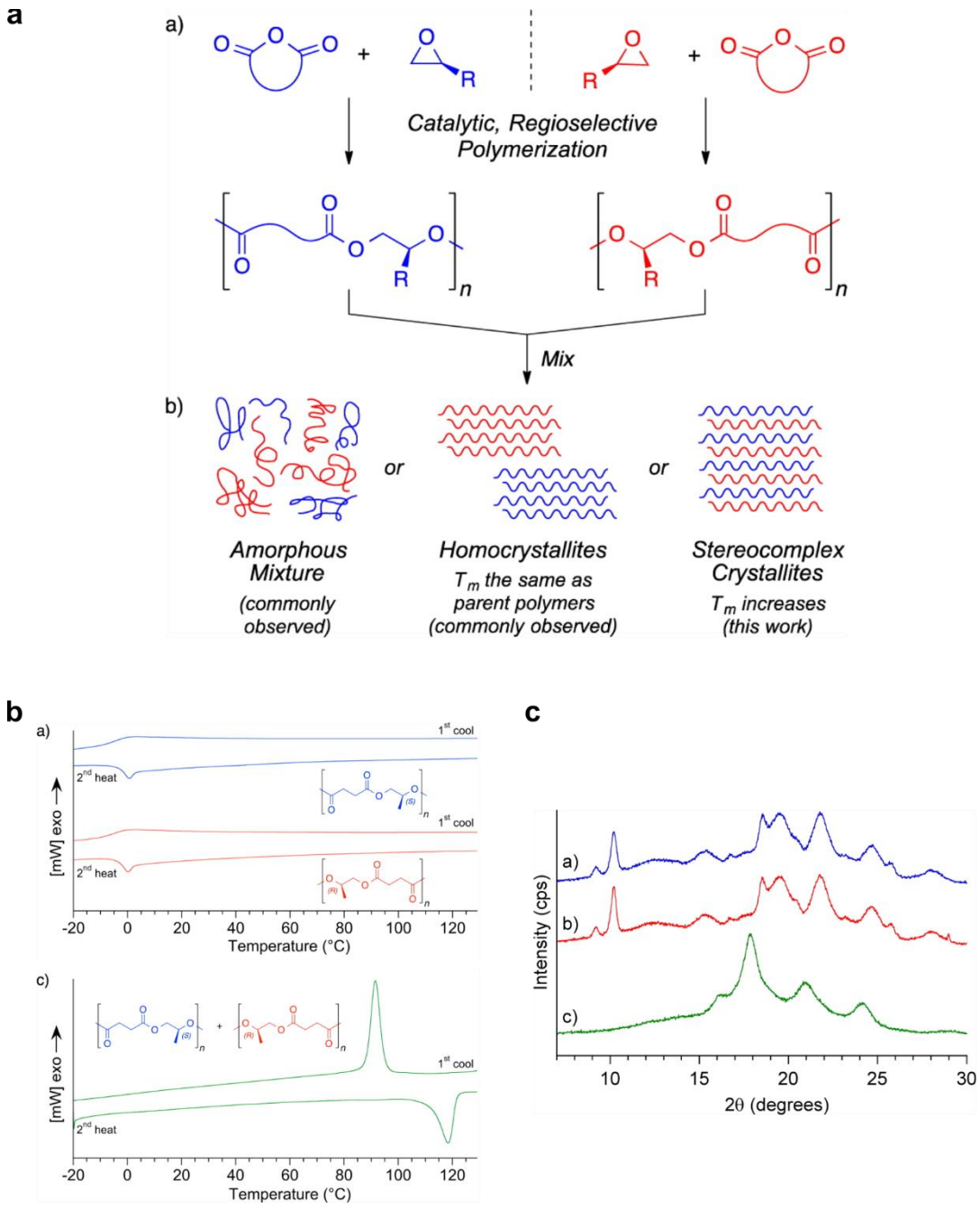

Figure 5. Stereocomplexation of poly(propylene succinate). (a) Structure of isotactic (*S*)- (blue) and (*R*)-poly(propylene succinate) (red) and illustration of formation of their stereocomplex. (b) DSC thermograms and (c) powder XRD patterns of the parent polymers (blue and red) and the stereocomplex (green). Reprinted with permission from ref. [32]. Copyright 2018 American Chemical Society.

II. Experimental Section

2.1 Synthesis and characterization of isotactic PAHGEs

Materials

All reagents and solvents were purchased from Thermo Fisher Scientific (Alfa Aesar) or Sigma-Aldrich and used as received unless otherwise stated. Deuterated NMR solvent, $CDCl_3$, was purchased from Cambridge Isotope Laboratories.

Characterization

^1H NMR and ^{13}C NMR were acquired using a 400-MR DD2 spectrometer at 400 MHz and 100 MHz respectively. All spectra were recorded in ppm units after being referenced to the residual peaks of $CDCl_3$. The number (M_n) and weight average molecular weight (M_w) and dispersity (M_w/M_n) were measured by gel permeation chromatography (GPC, Agilent Technologies 1200 series). Measurements in DMF were carried out at 40 °C with a flow rate of 1.0 mL/min using PMMA as a standard.

Synthesis

6-azido-1-hexanol. The precursor, 6-azido-1-hexanol, was synthesized through S_N2 reactions between the azide ion and chloride. A solution of 6-chloro-1-hexanol (14.23 mL, 107.28 mmol) and sodium azide (13.95 g, 214.61 mmol) in water (134 mL) was stirred under reflux for 24 h. After being cooled to room temperature, the reaction mixture was extracted with ethyl acetate and washed with water and brine. The organic layer was dried over anhydrous magnesium sulfate and concentrated under reduced pressure to give 6-azido-1-hexanol as a colorless liquid (13.99 g, 91%).

^1H NMR (400 MHz, chloroform-*d*): δ ppm 3.65 (td, J = 6.5, 4.9 Hz, –CH_2OH, 2H), 3.27 (t, J = 6.9 Hz, –CH_2N$_3$, 2H), 1.67 – 1.53 (m, –CH_2(CH$_2$)$_2$CH_2–, 4H), 1.47 – 1.34 (m, –(CH_2)$_2$–, 4H).

^{13}C NMR (101 MHz, chloroform-*d*): δ ppm 62.90 (–*C*H$_2$OH), 51.51 (–*C*H$_2$N$_3$), 32.68 (–*C*H$_2$CH$_2$OH), 28.94 (–*C*H$_2$CH$_2$N$_3$), 26.66 (–*C*H$_2$(CH$_2$)$_2$N$_3$), 25.47 (–*C*H$_2$(CH$_2$)$_2$OH).

(*S*)-AHGE monomer. 6-azido-1-hexanol (3.87 g, 27 mmol) was dissolved in a mixture of 50% aqueous sodium hydroxide solution (21.3 mL), benzene (21.3 mL) and tetrabutylammonium bromide (0.87 g, 3 mmol). (*S*)-Epichlorohydrin (5.00 g, 54 mmol) was added at 0 °C and the solution was stirred at room temperature for 17 h. The reaction mixture was extracted with ethyl acetate and washed several times with saturated aqueous sodium bicarbonate solution, water and brine. The organic layer was dried over anhydrous magnesium sulfate and concentrated under reduced pressure. The crude product was purified by silica gel flash column chromatography in hexane/diethyl ether 4:1.

The purified product was further dried under reduced pressure at 60 °C for at least 15 h to give (*S*)-AHGE monomer as a pale-yellow liquid (3.58 g, 67%).

^{1}H NMR (400 MHz, chloroform-*d*): δ ppm 3.72 (dd, J = 11.5, 3.0 Hz, –CHCH_2O–, 1H), 3.56–3.43 (m, –OCH_2CH$_2$–, 2H), 3.37 (dd, J = 11.5, 5.9 Hz, –CHCH_2O–, 1H), 3.27 (t, J = 6.9 Hz, –CH_2N$_3$–, 2H), 3.15 (ddt, J = 5.8, 4.2, 2.9 Hz, –C*H*–, 1H), 2.80 (dd, J = 5.0, 4.1 Hz, –CH_2OCH–, 1H), 2.61 (dd, J = 5.0, 2.7 Hz, –CH_2OCH–, 1H), 1.61 (m, –CH_2(CH$_2$)$_2$CH_2–, 4H), 1.46–1.35 (m, –(CH_2)$_2$–, 4H).

^{13}C NMR (101 MHz, chloroform-*d*): δ ppm 71.60 (–CH*C*H$_2$O–), 71.48 (–O*C*H$_2$CH$_2$–), 51.47 (–*C*H$_2$N$_3$), 50.97 (–*C*H–), 44.36 (–*C*H$_2$OCH–), 29.63 (–OCH$_2$*C*H$_2$–), 28.88 (–*C*H$_2$CH$_2$N$_3$–), 26.63 (–*C*H$_2$(CH$_2$)$_2$N$_3$), 25.78 (–O(CH$_2$)$_2$*C*H$_2$–).

ESI-MS: *m/z* calculated for $C_9H_{17}N_3O_2$ $[M+Na]^+$ 222.18, found 222.24.

(*R*)-AHGE monomer. (*R*)-AHGE monomer was synthesized in the same way from (*S*)-AHGE monomer except for using (*R*)-epichlorohydrin instead of (*S*)-epichlorohydrin. (59%).

ESI-MS: *m/z* calculated for $C_9H_{17}N_3O_2$ $[M+Na]^+$ 222.18, found 222.3.

Isotactic (*S*)-PAHGE (entry 1 in Table 1). A typical protocol is as follows (Protocol A). A 50 mL Schlenk tube was flame-dried under vacuum and flushed with nitrogen for three times. *t*-Bu-P$_4$ (0.16 mL as a 0.80 M stock solution in hexane, 0.13 mmol) was added to a solution of benzyl alcohol (0.13 mL as a 1.0 M stock solution in toluene, 0.13 mmol) as an initiator in toluene (1.50 mL). A few minutes later (*S*)-AHGE monomer (0.65 g, 3.26 mmol) was added and the solution was stirred at room temperature. The polymerization was quenched by the addition of benzoic acid after the full consumption of the monomer as monitored by ^{1}H NMR. The mixture was passed through a pad of basic alumina with THF. The eluate was concentrated under reduced pressure, which was then precipitated in hexane to give isotactic (*S*)-PAHGE as a cloudy oil (190 mg, 29%).

^{1}H NMR (400 MHz, chloroform-*d*): δ ppm 7.35–7.30 (m, aromatic), 4.54 (s, Ar CH_2–, 2H), 3.70–3.35 (m, backbone), 3.27 (dd, –CH_2N$_3$), 1.67–1.49 (m, –CH_2(CH$_2$)$_2$CH_2–), 1.38 (m, –(CH_2)$_2$–).

$M_{n.NMR}$ = 6,700 g/mol, $M_{n.GPC}$ = 2,980 g/mol, M_w/M_n = 1.10 in DMF.

Isotactic (*R*)-PAHGE (entry 4 in Table 1). (Protocol A) Polymerization using *t*-Bu-P$_4$ (0.30 mL as a 0.80 M stock solution in hexane, 0.24 mmol), benzyl alcohol (0.24 mL as a 1.0 M stock solution in toluene, 0.24 mmol) and (*R*)-AHGE monomer (1.2 g, 6.02 mmol) in toluene (2.40 mL) gave isotactic (*R*)-PAHGE as a pale-yellow oil (493 mg, 41%).

$M_{n.NMR}$ = 5,700 g/mol, $M_{n.GPC}$ = 3,210 g/mol, M_w/M_n = 1.21 in DMF.

2.2 Investigation on stereocomplexation of the isotactic P(A)HGEs

Materials

All reagents and solvents were purchased from Thermo Fisher Scientific (Alfa Aesar) or Sigma-Aldrich and used as received unless otherwise stated. Deuterated NMR solvent, $CDCl_3$, was purchased from Cambridge Isotope Laboratories.

Characterization

^{1}H NMR and ^{13}C NMR were acquired using a 400-MR DD2 spectrometer at 400 MHz and 100 MHz respectively. All spectra were recorded in ppm units after being referenced to the residual peaks of $CDCl_3$. The M_n, M_w and M_w/M_n were measured by GPC (Agilent Technologies 1200 series). Measurements in DMF were carried out at 40 °C or in $CHCl_3$ at 30 °C with a flow rate of 1.0 mL/min using PMMA as a standard. Measurements in THF were carried out at 35 °C with a flow rate of 1.0 mL/min using PS as a standard. Differential scanning calorimetry (DSC) was performed using a differential scanning calorimeter (TA Instruments Q200 model) in the temperature range of -80 to 70 °C at heating or cooling rates of 10 °C/min under a nitrogen atmosphere.

Synthesis

Block copolymer (*R*)-PAHGE$_{13}$-*b*-(*S*)-PAHGE$_{14}$ (entry 4 in Table 2). A 50 mL Schlenk tube was flame-dried under vacuum and flushed with nitrogen for three times. *t*-Bu-P$_4$ (0.20 mL as a 0.80 M stock solution in hexane, 0.16 mmol) was added to a solution of benzyl alcohol (16.7 μL, 0.16 mmol) as an initiator in toluene (1.60 mL). A few minutes later (*R*)-AHGE monomer (0.44 g, 2.21 mmol) was added and the solution was stirred at room temperature. After the full consumption of the (*R*)-AHGE monomer, (*S*)-AHGE monomer (0.44 g, 2.21 mmol) was added for subsequent polymerization. The polymerization was quenched by the addition of benzoic acid after the full consumption of the second monomer as monitored by ^{1}H NMR. The mixture was passed through a pad of basic alumina with THF. The eluate was concentrated under reduced pressure, which was then precipitated in hexane to give the block copolymer (*R*)-PAHGE$_{13}$-*b*-(*S*)-PAHGE$_{14}$ as a yellow oil (461 mg, 52%).

^{1}H NMR (400 MHz, chloroform-*d*): δ ppm 7.33 (m, aromatic), 4.54 (s, Ar CH_2–, 2H), 3.75–3.37 (m, backbone), 3.27 (dd, –CH_2N$_3$), 1.70–1.51 (m, –CH_2(CH$_2$)$_2$CH_2–), 1.47–1.31 (m, –(CH_2)$_2$–).

$M_{n.NMR}$ = 5,500 g/mol, $M_{n.GPC}$ = 2,960 g/mol, M_w/M_n = 1.24 in DMF.

(*S*)-HGE monomer. 1-hexanol (6.28 mL, 100 mmol) was dissolved in a mixture of 50% aqueous sodium hydroxide solution (39.6 mL) and tetrabutylammonium bromide (1.61 g, 5 mmol). (*S*)-Epichlorohydrin (7.83 mL, 100 mmol) was added at 0 ℃ and the solution was stirred at room temperature for 17 h. The reaction mixture was extracted with ethyl acetate and washed several times

with saturated aqueous sodium bicarbonate solution, water and brine. The organic layer was dried over anhydrous magnesium sulfate and concentrated under reduced pressure. The crude product was purified by silica gel flash column chromatography in hexane/diethyl ether 4:1 to give (*S*)-HGE monomer as a clear liquid (4.17 g, 53%).

^{1}H NMR (400 MHz, chloroform-*d*): δ ppm 3.70 (dd, J = 11.5, 3.1 Hz, –CHCH_2O–, 1H), 3.49 (qt, J = 9.2, 6.7 Hz, –OCH_2CH$_2$–, 2H), 3.39 (dd, J = 11.5, 5.8 Hz, –CHCH_2O–, 1H), 3.15 (ddt, J = 5.8, 4.2, 2.9 Hz, –C*H*–, 1H), 2.80 (dd, J = 5.0, 4.1 Hz, –CH_2OCH–, 1H), 2.61 (dd, J = 5.1, 2.7 Hz, –CH_2OCH–, 1H), 1.67–1.53 (m, –OCH$_2$CH_2–, 2H), 1.41–1.22 (m, –(CH_2)$_3$CH$_3$, 6H), 0.95–0.83 (m, –CH_3, 3H).

^{13}C NMR (101 MHz, chloroform-*d*): δ ppm 71.89 (–CH*C*H$_2$O–), 71.61 (–O*C*H$_2$CH$_2$–), 51.06 (–*C*H–), 44.50 (–*C*H$_2$OCH–), 31.83 (–O(CH$_2$)$_2$*C*H$_2$–), 29.82 (–OCH$_2$*C*H$_2$–), 25.91 (–*C*H$_2$CH$_2$CH$_3$), 22.76 (–*C*H$_2$CH$_3$), 14.18 (–*C*H$_3$).

ESI-MS: *m/z* calculated for $C_9H_{18}O_2$ [M+Na]$^+$ 181.18, found 181.12.

(*R*)-HGE monomer. (*R*)-HGE monomer was synthesized in the same way from (*S*)-HGE monomer except for using (*R*)-epichlorohydrin instead of (*S*)-epichlorohydrin. (5.01 g, 63%).

ESI-MS: *m/z* calculated for $C_9H_{18}O_2$ [M+Na]$^+$ 181.18, found 181.12

Isotactic (*S*)-PHGE (entry 2 in Table 4). A typical protocol is as follows (Protocol A). A 50 mL Schlenk tube was flame-dried under vacuum and flushed with nitrogen for three times. *t*-Bu-P$_4$ (0.13 mL as a 0.80 M stock solution in hexane, 0.10 mmol) was added to a solution of benzyl alcohol (10.6 μL, 0.10 mmol) as an initiator in toluene (0.63 mL). A few minutes later (*S*)-HGE monomer (0.50 g, 3.16 mmol) was added and the solution was stirred at room temperature. The polymerization was quenched by the addition of benzoic acid after the full consumption of the monomer as monitored by ^{1}H NMR. The mixture was passed through a pad of basic alumina with THF. The eluate was concentrated under reduced pressure, which was then precipitated in hexane to give isotactic (*S*)-PHGE as a pale-yellow self-standing gel (435 mg, 87%).

^{1}H NMR (400 MHz, chloroform-*d*): δ ppm 7.33 (m, aromatic), 4.54 (s, Ar CH_2–, 2H), 3.73–3.30 (m, backbone), 1.60–1.47 (m, –CH_2(CH$_2$)$_3$CH$_3$), 1.41–1.20 (m, –CH$_2$(CH_2)$_3$CH$_3$), 0.97–0.80 (m, –CH$_3$).

$M_{n.NMR}$ = 6,000 g/mol, $M_{n.GPC}$ = 5,000 g/mol, M_w/M_n = 1.08 in THF.

Isotactic (*R*)-PHGE (entry 3 in Table 4). (Protocol A) Polymerization using *t*-Bu-P$_4$ (0.13 mL as a 0.80 M stock solution in hexane, 0.10 mmol), benzyl alcohol (10.6 μL, 0.10 mmol) and (*R*)-HGE monomer (0.50 g, 3.16 mmol) in toluene (0.63 mL) gave isotactic (*R*)-PHGE as a pale-yellow oil (406 mg, 81%).

$M_{n.NMR}$ = 6,800 g/mol, $M_{n.GPC}$ = 5,580 g/mol, M_w/M_n = 1.07 in THF.

Atactic (*rac.*)-PHGE (entry 1 in Table 4). (Protocol A) Polymerization using *t*-Bu-P_4 (0.13 mL as a 0.80 M stock solution in hexane, 0.10 mmol), benzyl alcohol (10.6 μL, 0.10 mmol) and 1:1 mixture of (*S*)- and (*R*)-HGE monomer (0.50 g, 3.16 mmol in total) in toluene (0.63 mL) gave atactic (*rac.*)-PHGE as a pale-yellow oil (421 mg, 84%).

$M_{n.NMR}$ = 6,400 g/mol, $M_{n.GPC}$ = 5,430 g/mol, M_w/M_n = 1.06 in THF.

Other preparation

1:1 polymer blend. First, 20 mg of completely dried polymer was each dissolved in a minimal but the same amount of chloroform. The same portion of two solution was taken to be mixed in another 4 mL vial. The final solution was left for evaporation of chloroform in the air and further dried under vacuum for at least 1 day. Chloroform was selected because of its volatility.

III. Results and Discussion

3.1 Synthesis and characterization of isotactic PAHGEs

The designed AHGE monomer was synthesized via two-step synthesis (Figure 6 (a)). First, azido moieties which is well known as a versatile platform for post-modification such as (copper-catalyzed) azide-alkyne cycloaddition or photo-crosslinking upon UV-irradiation (250 to 350 nm) was introduced by azidation on chloride of 6-chloro-1-hexanol (Figure 7). The 6-azido-1-hexanol was then reacted with epichlorohydrin to obtain the azido-functionalized epoxide monomer. The chirality of AHGE monomer was determined by that of the chiral precursor epichlorohydrin, so both (*S*) and (*R*)-AHGE monomers were easily prepared. The successful synthesis of the AHGE monomer was confirmed by ^{1}H and ^{13}C NMR spectroscopy (Figure 8).

After the successful synthesis of AHGE monomer, AROP was performed using benzyl alcohol as an initiator and *t*-Bu-P$_4$ as a base (Figure 6 (b)). The strong organic base *t*-Bu-P$_4$ (pK_a = 30.2 in DMSO) allowed deprotonation of benzyl alcohol and subsequent polymerization of the AHGE monomers at room temperature. As the polymerization proceeded, the monomer conversion was monitored by ^{1}H NMR spectroscopy with a disappearance of epoxide ring peak at 3.72, 3.56–3.43, 3.37 and 3.15 ppm and simultaneous appearance of a broad peak at 3.70–3.35 ppm which is attributed to protons on polyether backbone. Every monomer was converted typically within 1 day to yield the homopolymers after the filtration of *t*-Bu-P$_4$ indicated by clear removal of the corresponding peak at 2.7 ppm (Figure 9, from (b) to (c)). As shown in Figure 11, characteristic peaks of hydroxyl group and azide group on FT-IR spectra well agreed with the whole synthetic procedure from 6-chloro-1-hexanol to the final (*S*)-PAHGE. The polymerization of each of the (*S*)- and (*R*)-AHGE monomer afforded isotactic PAHGEs respectively.

Isotactic PAHGEs with various molecular weight (5,000, 10,000 and 20,000 g/mol) were prepared by changing monomer-to-initiator ratios from 25, 50 to 100. All polymers were characterized by ^{1}H, ^{13}C NMR and GPC (Table 1). The number average molecular weight calculated from the ^{1}H NMR spectra ($M_{n.NMR}$) by end-group analysis was close to the target value. For example, degree of polymerization (DP) of (*S*)-PAHGE$_{33}$ (entry 1 in Table 1) was calculated from the ratio of peak areas between the peak assigned to methylene group of benzyl alcohol (4.54 ppm, 2H) and polyether backbone (3.70–3.35 ppm, DP × 7H) or methylene group nearby azide group on each side chain (3.27 ppm, DP × 2H) (Figure 10 (a)); $M_{n.NMR}$ = 108.14 (molecular weight of benzyl alcohol) + 199.25 (molecular weight of the AHGE monomer) × 33 = 6,683.39 g/mol ≈ 6,700 g/mol.

To confirm the tacticity of the prepared PAHGEs, ^{13}C NMR spectroscopy was used for tacticity analysis. The methine carbon peak region (79.0 ppm) on the NMR spectrum was expanded to observe the resonance. However, as shown in Table 1 and Figure 12, all of the PAHGEs predicted to be

isotactic turned out to be 80% isotactic in average. The possible reason for lacking the 100% isotacticity is the chiral monomer lacking the enantiopurity. Both enantiopure monomer and regioselective ring opening during the polymerization are necessary to realize the isotactic sequence.[34] Isono *et al.* already reported the successful synthesis of the isotactic polymers from the various chiral epoxide monomers without stereoinversion in *t*-Bu-P_4-catalyzed AROP only if the monomer is optically-pure.[14,19,20] %*ee* (enantiomeric excess) which indicates the enantiopurity can be determined using chiral HPLC (high performance liquid chromatography), but the values of (*S*)- and (*R*)-AHGE monomers here have not been measured yet. Further steps were taken keeping the lacking isotacticity of the PAHGEs in mind, although it may hamper a clear conclusion of this study.

In addition, GPC traces of the PAHGEs using PMMA as a standard in DMF showed no tendency (Table 1 and Figure 13). The $M_{n.GPC}$ values were always lower than the $M_{n.NMR}$, but did not consistently increase along with the increasing $M_{n.NMR}$. For (*S*)-PAHGEs (entry 1–3), the $M_{n.GPC}$ of $PAHGE_{49}$ (entry 2) was larger than that of $PAHGE_{33}$ (entry 1) but was also larger than that of $PAHGE_{100}$ (entry 3). For (*R*)-PAHGEs (entry 4–6), the $M_{n.GPC}$ of $PAHGE_{52}$ (entry 5) was smaller than that of $PAHGE_{28}$ (entry 4). $PAHGE_{216}$ (entry 6) eventually showed the largest $M_{n.GPC}$ albeit the high dispersity and a shoulder peak on its trace. This abnormal behavior led us to mix two enantiomeric chains, i.e. (*S*)-$PAHGE_{33}$ and (*R*)-$PAHGE_{28}$ (Figure 14). The sample was prepared as follows. First, each polymer was dissolved in DMF (1.5 mg/mL) and different portion of two solutions according to desired fraction were taken to be mixed well to give a total of 2 mL of solution. The final solution was filtered through syringe filter before the measurement. Interestingly, when they were mixed in varying fractions, the $M_{n.GPC}$s were all similar but decreased only when the fraction of (*R*)-$PAHGE_{28}$ is 0.5 which means the amount of two enantiomeric chains is identical. The result possibly implied the existence of stereoselective interactions while it was still suspicious due to the fact that GPC gives not absolute but relative information on molecular weight based on hydrodynamic volume.

In summary, the synthesis of the chiral AHGE monomers and the resulting isotactic PAHGEs were introduced in section 3.1. The *t*-BuP_4-catalyzed AROP successfully afforded a series of PAHGEs with different molecular weights, but the polymers were not perfectly isotactic which was differ from the previously reported papers. It may due to relatively lower enantiopurity of the chiral AHGE monomers and %*ee* values have to be determined first of all. However, GPC characterization of the mixture of two enantiomeric polymers suggested that the stereoselective interactions may occur at the specific ratio. Therefore, further investigations on the phenomenon were made and introduced in the next section.

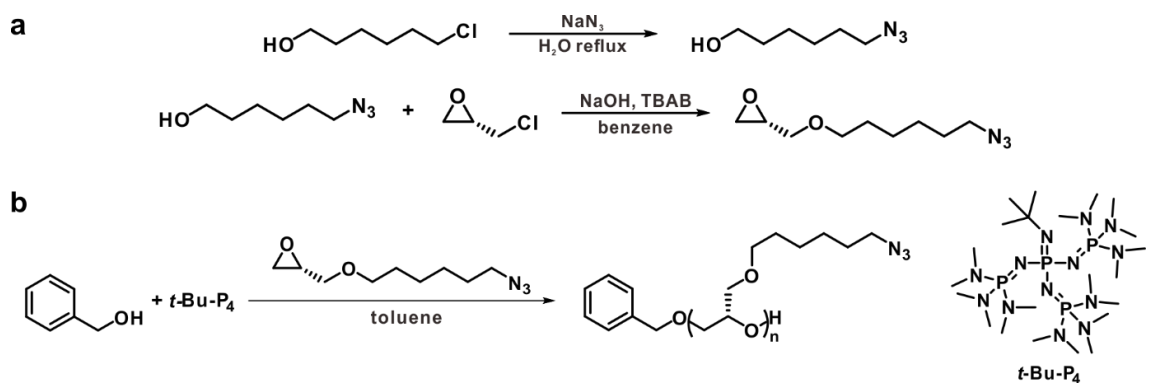

Figure 6. Synthetic scheme of (a) the (*S*)-AHGE monomer and (b) the (*S*)-PAHGE.

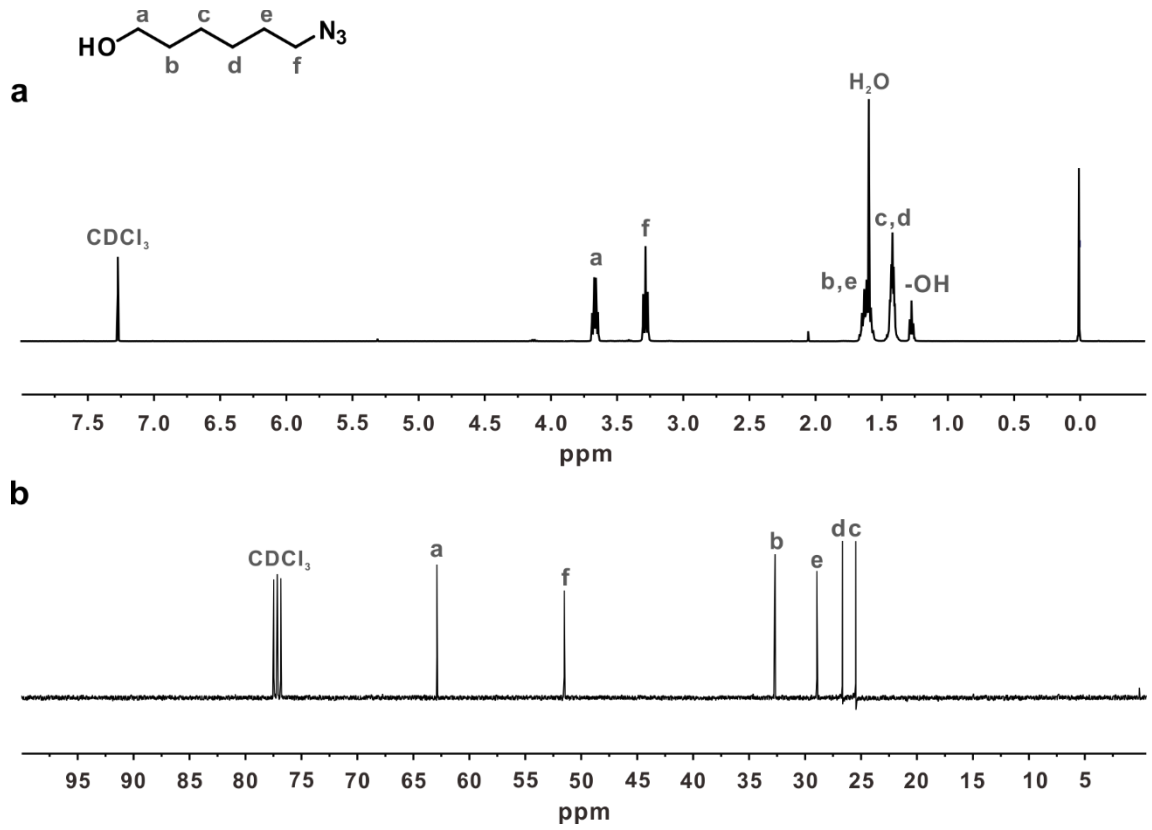

Figure 7. Representative (a) ^{1}H and (b) ^{13}C NMR spectrum of the 6-azido-1-hexanol.

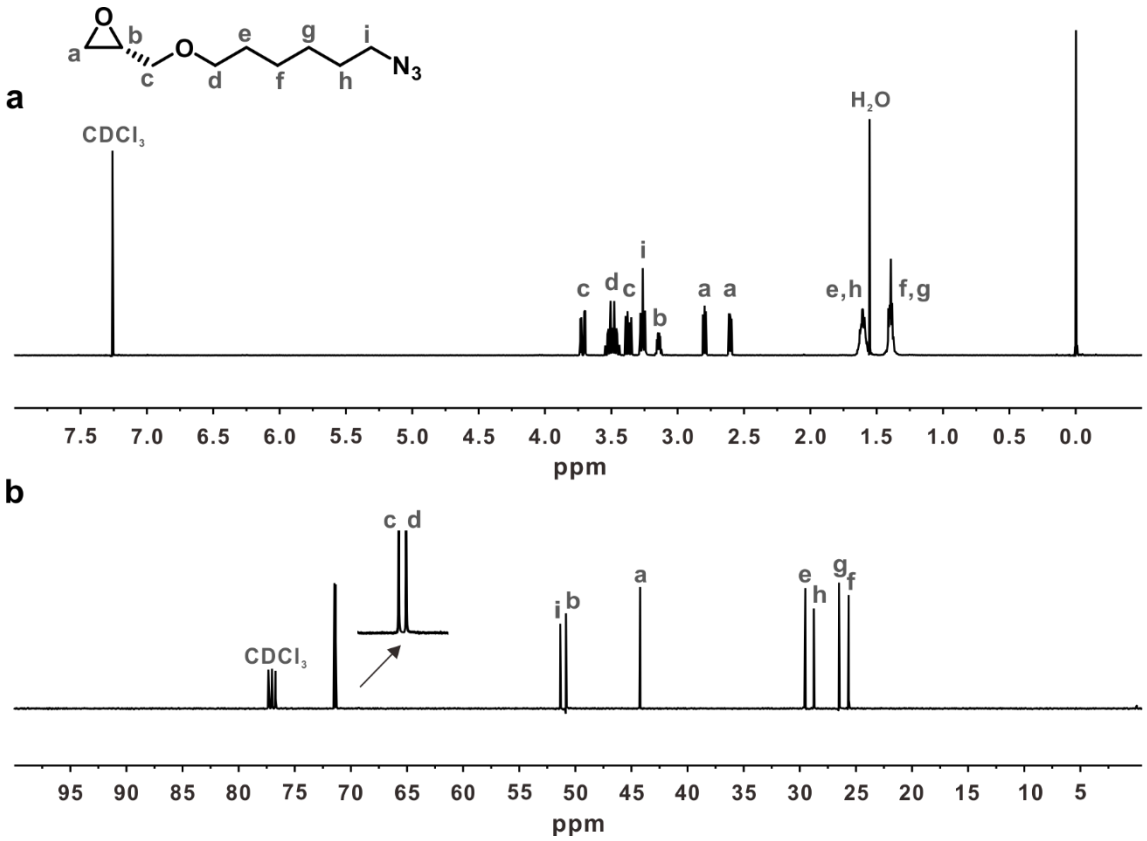

Figure 8. Representative (a) ^{1}H and (b) ^{13}C NMR spectrum of the (*S*)-AHGE monomer.

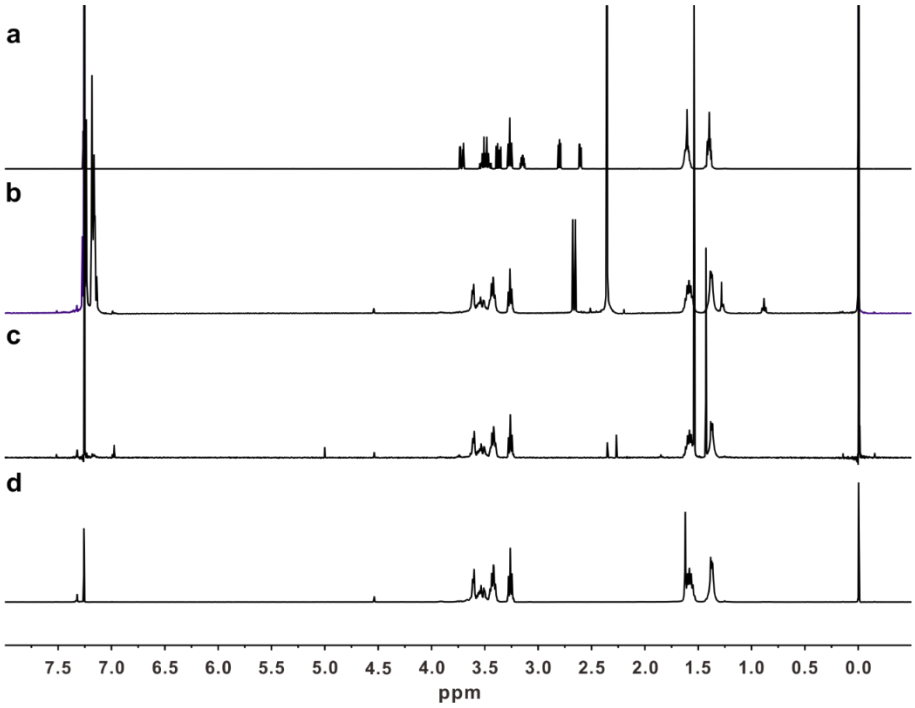

Figure 9. Representative ^{1}H NMR spectra (a) of the (*S*)-AHGE monomer, (b) taken after the full monomer conversion, (c) taken after *t*-Bu-P_4 filtration and (d) of the final PAHGE (entry 1 in Table 1).

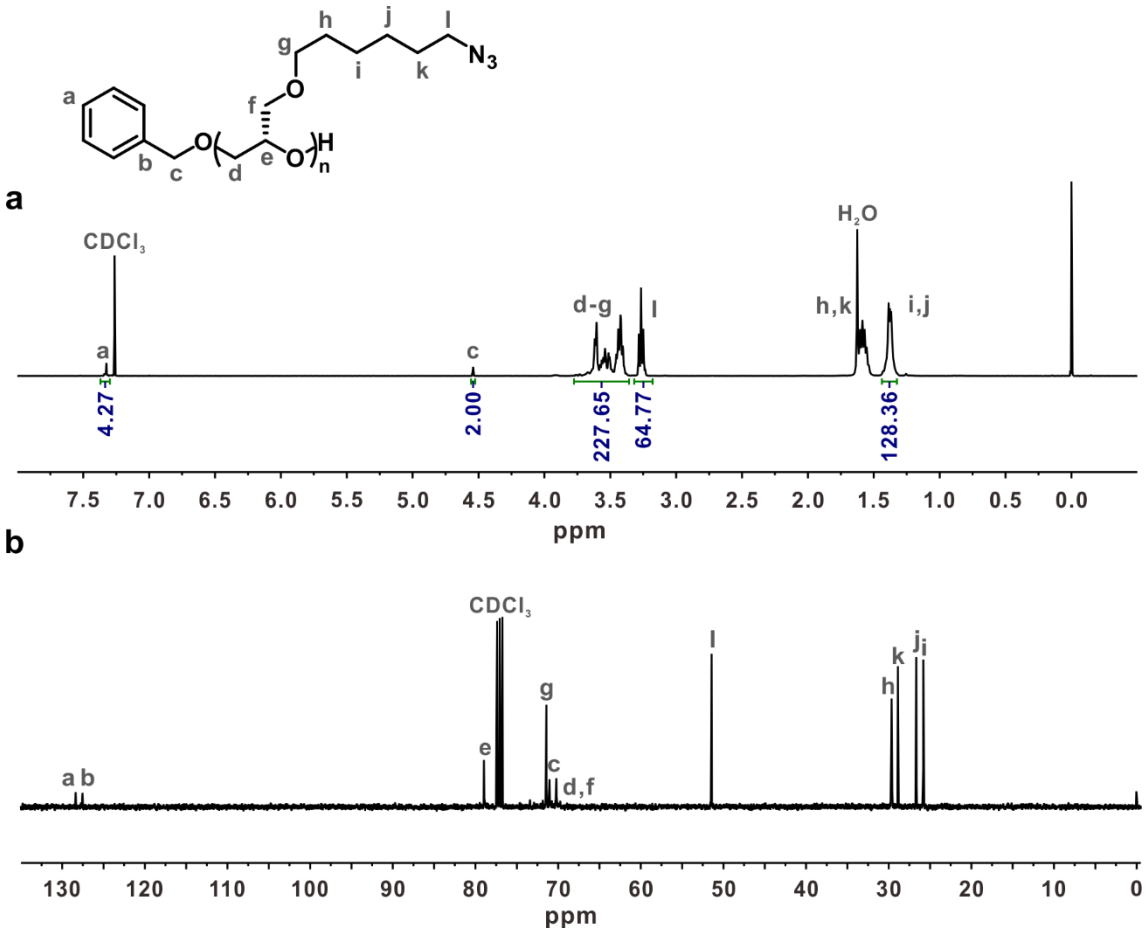

Figure 10. Representative (a) ^{1}H and (b) ^{13}C NMR spectrum of the (*S*)-$PAHGE_{33}$ (entry 1 in Table 1).

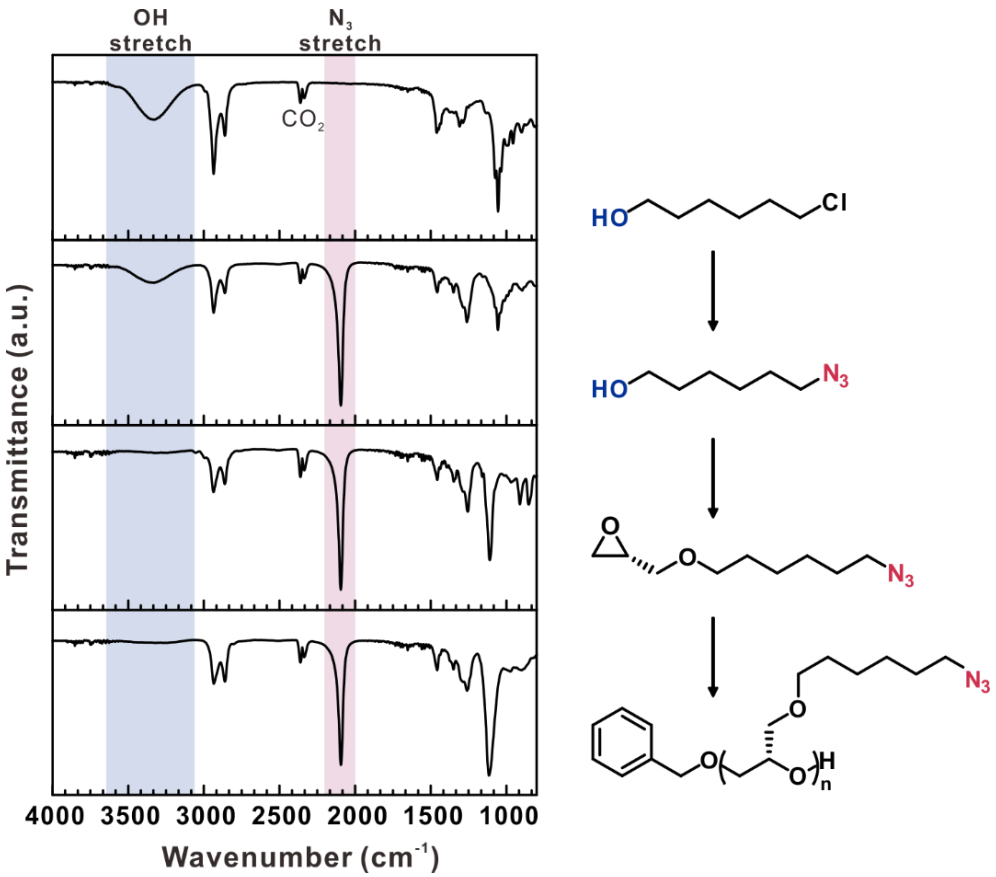

Figure 11. FT-IR spectra of the products in each step.

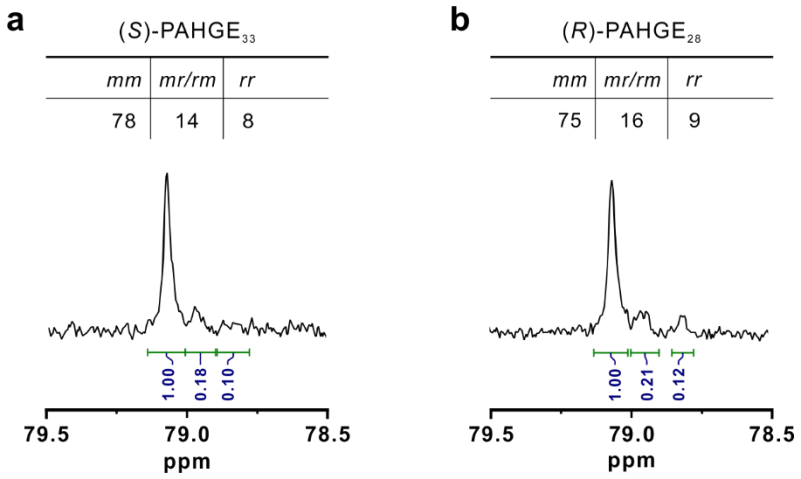

Figure 12. Representative expanded ^{13}C NMR spectra of (a) (*S*)-PAHGE$_{33}$ and (b) (*R*)-PAHGE$_{28}$ for tacticity analysis.

Table 1. Characterization data for PAHGEs.

Entry		Polymer composition (NMR)	M_n (^{1}H NMR, g/mol)	M_n[a] (GPC, g/mol)	M_w/M_n[a] (GPC)	[mm] [b] (^{13}C NMR, %)
1		$PAHGE_{33}$	6,700	2,980	1.10	78
2	(S)	$PAHGE_{49}$	9,900	4,790	1.29	80
3		$PAHGE_{100}$	20,000	3,890	1.22	84
4		$PAHGE_{28}$	5,700	3,210	1.21	75
5	(R)	$PAHGE_{52}$	10,500	2,390	1.23	81
6		$PAHGE_{216}$	43,000	6,760	1.34	90

[a] Determined by GPC (eluent: DMF, calibration: PMMA). [b] Determined by ^{13}C NMR (from methine peak at 79.0 ppm).

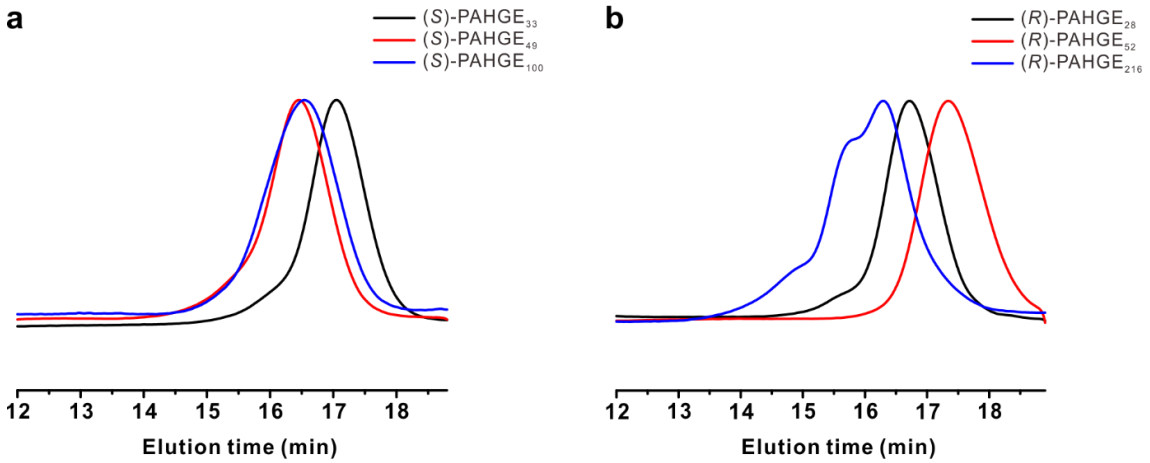

Figure 13. GPC traces of (a) (*S*)-PAHGEs and (b) (*R*)-PAHGEs (eluent: DMF, calibration: PMMA).

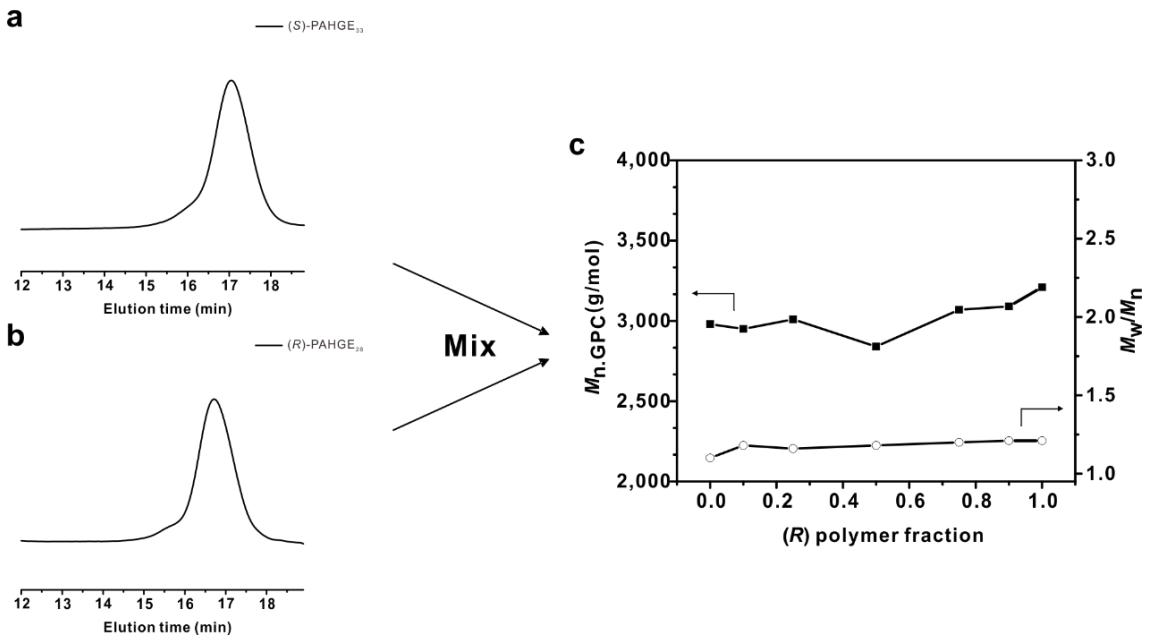

Figure 14. GPC traces of (a) (*S*)-$PAHGE_{33}$, (b) (*R*)-$PAHGE_{28}$ and (c) $M_{n.GPC}$ (left) and M_w/M_n (right) for their mixtures at varying fractions.

3.2 Investigation on stereocomplexation of the isotactic P(A)HGEs

To elucidate the origin of the abnormal behavior shown in the section 3.1, first of all, the reproducibility was checked. The polymers with the same composition were newly synthesized because of their low stability during storage (data not shown). Characterization data for all PAHGEs newly synthesized are shown in Table 2. Here, in particular, the block copolymer of an equal length of (*R*)-PAHGE$_{13}$ and (*S*)-PAHGE$_{14}$ was synthesized as a control to study whether the same phenomenon would occur when (*S*)- and (*R*)-entities exist on the same block, not separately. The clear shift of GPC trace after the second polymerization confirmed the successful synthesis of the block copolymer (Figure 15).

Nevertheless, the phenomenon was not reproducible; the GPC traces of the newly synthesized PAHGEs shifted to the shorter time region as the $M_{n.NMR}$ values increased for both (*S*)- (entry 1-3) and (*R*)-PAHGEs (entry 5-7) (Figure 16). The characteristic decrease when two enantiomeric polymers were mixed was also absent as shown in Figure 17. Instead, the $M_{n.GPC}$s gradually shifted from that of pure (*S*)-PAHGE where (*R*)-PAHGE fraction is zero, to that of pure (*R*)-PAHGE where the fraction is one. The $M_{n.GPC}$ of the block copolymer (entry 4) was also similar to the case where (*R*)-PAHGE fraction is 0.5. The values mostly agreed with the numerically calculated ones except for the pair of (*S*)-PAHGE$_{31}$ and (*R*)-PAHGE$_{25}$ with $M_{n.NMR}$ around 5,000 g/mol. The *R*-square coefficient of the linear trend line was 0.84 for the pair of (*S*)-PAHGE$_{49}$ and (*R*)-PAHGE$_{49}$ (around 10,000 g/mol) and 0.95 for the pair of (*S*)-PAHGE$_{100}$ and (*R*)-PAHGE$_{98}$ (around 20,000 g/mol). It highlights that there is no stereoselective interaction between two polymers. In other words, the mixture is mere a blend rather than the stereocomplex.

The samples were then subjected to GPC characterization using chloroform as eluent as well. Chloroform is nonpolar in contrast to polar DMF. It has been known that solvent affects stereocomplexation by interacting with functional groups of polymers. The solvent which could promote molecular rearrangement to induce stereocomplexation is called complexing solvent. The solvent which disassembles the inclusion complex is non-complexing solvent, in opposite. The same solvent may bring different effects depending on polymer types. For instance, the complexing solvent of PMMA stereocomplex includes acetone and DMF.[21] Chloroform or dichloromethane are the non-complexing solvent for PMMA stereocomplex, but suitable for the case of PLA.[30,31] However, the GPC characterization gave the similar result (Table 3 and Figure 19) further denying the stereocomplexation of PAHGEs.

Afterward, the polymers and 1:1 blends of each polymer with similar molecular weights underwent DSC measurement to investigate crystallinities. As shown in Figure 20 and Figure 21, not only an atactic PAHGE synthesized from the racemic AHGE monomer in our laboratory but also isotactic PAHGEs were amorphous regardless of their molecular weight. In some case, such as (*S*)-PAHGE$_{31}$

(Figure 20 (b)), (*R*)-PAHGE$_{25}$ (Figure 20 (c)) and (*S*)-PAHGE$_{100}$ (Figure 21 (d)), endothermic peak was observed around at 0 °C. However, those peaks are not attributed to the glass transition from the fact that the glass transition temperature (T_g) of liquid glycidyl azide polymers is known as -45 to -40 °C.[35,36] Bulky pendant groups lower the T_g, so T_g of our PAHGEs with hexyl spacer on the side chain may not be observed above -80 °C. Although the imperfect isotacticity would affect the crystallinity, by Brochu *et al.* it was reported that even isotactic glycidyl azide polymers lacked the crystallinity.[37] They synthesized the isotactic glycidyl azide polymers through the azidation of isotactic and crystalline poly(epichlorohydrin)s, but the crystallinity disappeared after the process. Thus, the authors concluded that it was because azide group is larger and less electronegative than chlorine atom on poly(epichlorohydrin)s.

From the GPC and DSC measurements, the isotactic PAHGEs turned out not to form stereocomplex in our study. The DSC measurements further revealed that azide moieties originally introduced for the post-modification afterward hindered the chain packing to result in amorphous PAHGEs irrespective of their tacticity. As the crystallinity indicates some tacticity, we tried to modify the designed azidohexyl glycidyl ether (AHGE) monomer to hexyl glycidyl ether (HGE) monomer; to observe whether crystallinity arises in isotactic polymer and the effect of azide group.

Table 2. Characterization data for PAHGEs.

Entry		Polymer composition (NMR)	M_n (^{1}H NMR, g/mol)	M_n[a] (GPC, g/mol)	M_w/M_n[a] (GPC)	[mm] [b] (^{13}C NMR, %)
1		$PAHGE_{31}$	6,300	2,790	1.15	72
2	(S)	$PAHGE_{49}$	9,900	3,420	1.29	83
3		$PAHGE_{100}$	20,000	4,120	1.26	84
4	(R)→(S)	$PAHGE_{27}$	5,500	2,960	1.24	61
5		$PAHGE_{25}$	5,100	2,950	1.24	73
6	(R)	$PAHGE_{49}$	9,900	3,970	1.35	71
7		$PAHGE_{98}$	19,600	4,970	1.42	61

[a] Determined by GPC (eluent: DMF, calibration: PMMA). [b] Determined by ^{13}C NMR (from methine peak at 79.0 ppm).

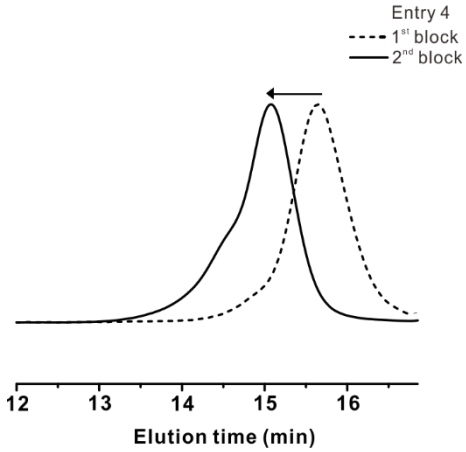

Figure 15. GPC traces of the block copolymer $PAHGE_{27}$ (entry 4 in Table 2) after the first polymerization (dash) and the second polymerization (solid).

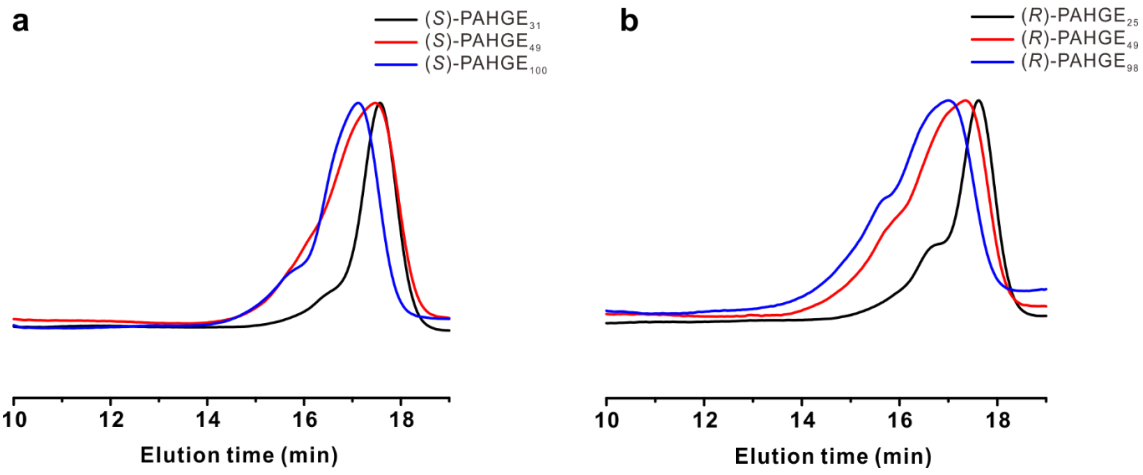

Figure 16. GPC traces of (a) (*S*)-PAHGEs and (b) (*R*)-PAHGEs (eluent: DMF, calibration: PMMA).

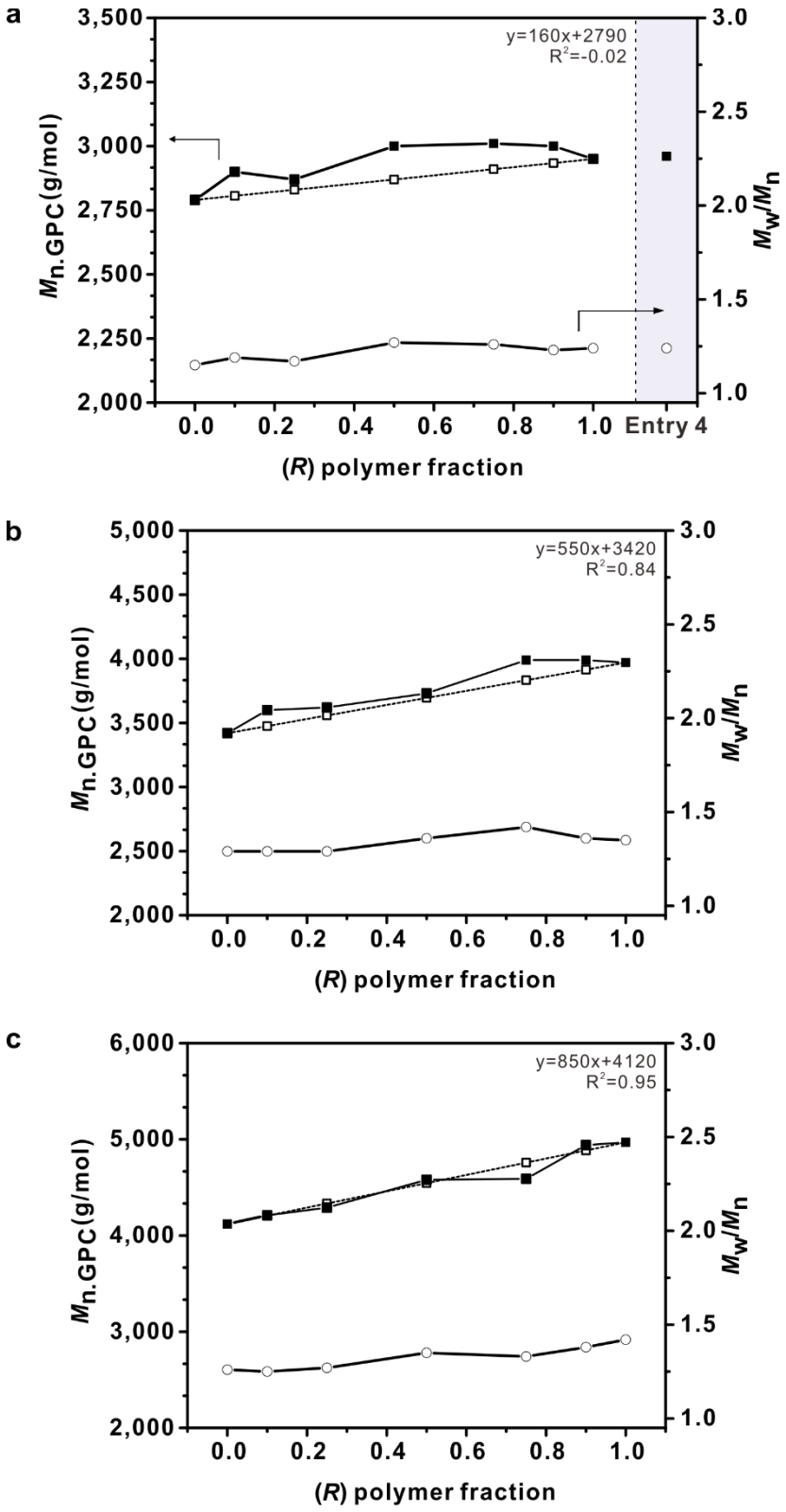

Figure 17. $M_{n.GPC}$ (left) and M_w/M_n (right) measured in DMF for the mixtures of (a) (*S*)-PAHGE$_{31}$/(*R*)-PAHGE$_{25}$, (b) (*S*)-PAHGE$_{49}$/(*R*)-PAHGE$_{49}$ and (c) (*S*)-PAHGE$_{100}$/(*R*)-PAHGE$_{98}$ at varying fractions.

Table 3. Characterization data for PAHGEs.

Entry		Polymer composition (NMR)	M_n (^{1}H NMR, g/mol)	M_n[a] (GPC, g/mol)	M_w/M_n[a] (GPC)	[mm] [b] (^{13}C NMR, %)
1		$PAHGE_{31}$	6,300	5,420	1.15	72
2	(S)	$PAHGE_{49}$	9,900	6,560	1.23	83
3		$PAHGE_{100}$	20,000	9,550	1.25	84
4	(R)→(S)	$PAHGE_{27}$	5,500	5,530	1.23	61
5		$PAHGE_{25}$	5,100	5,700	1.14	73
6	(R)	$PAHGE_{49}$	9,900	7,680	1.29	71
7		$PAHGE_{98}$	19,600	7,490	1.27	61

[a] Determined by GPC (eluent: $CHCl_3$, calibration: PMMA). [b] Determined by ^{13}C NMR (from methine peak at 79.0 ppm).

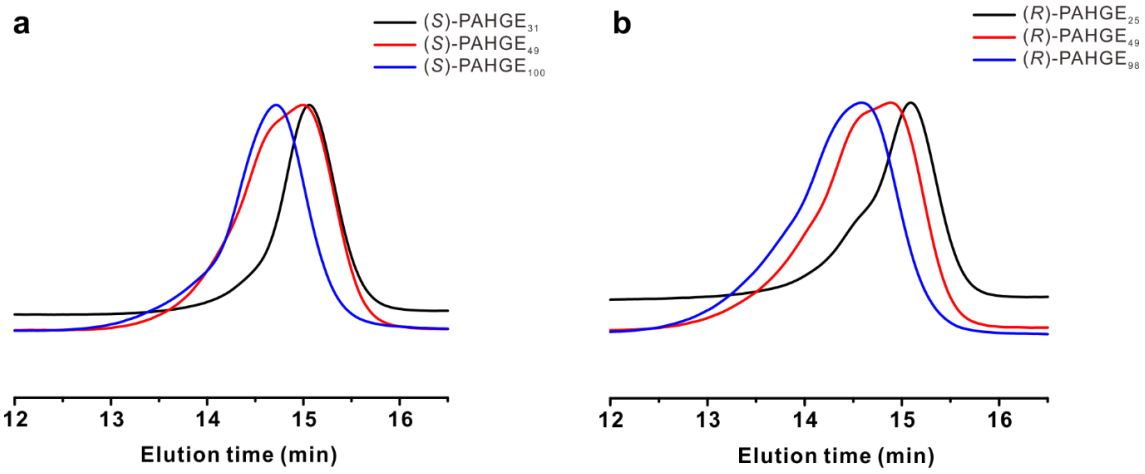

Figure 18. GPC traces of (a) (*S*)-PAHGEs and (b) (*R*)-PAHGEs (eluent: $CHCl_3$, calibration: PMMA).

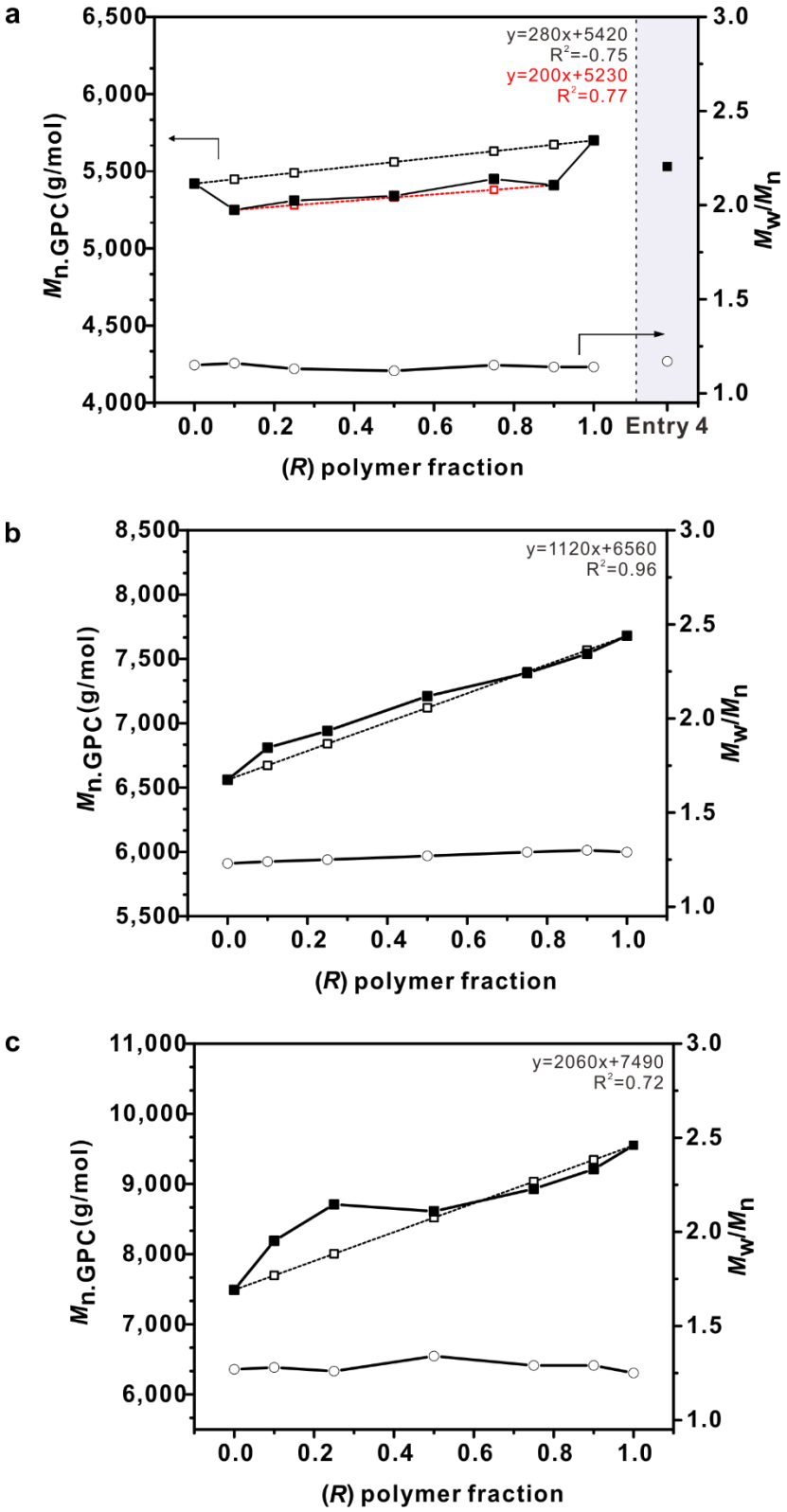

Figure 19. $M_{n.GPC}$ (left) and M_w/M_n (right) measured in $CHCl_3$ for the mixtures of (a) (*S*)-PAHGE$_{31}$/(*R*)-PAHGE$_{25}$, (b) (*S*)-PAHGE$_{49}$/(*R*)-PAHGE$_{49}$ and (c) (*S*)-PAHGE$_{100}$/(*R*)-PAHGE$_{98}$ at varying fractions.

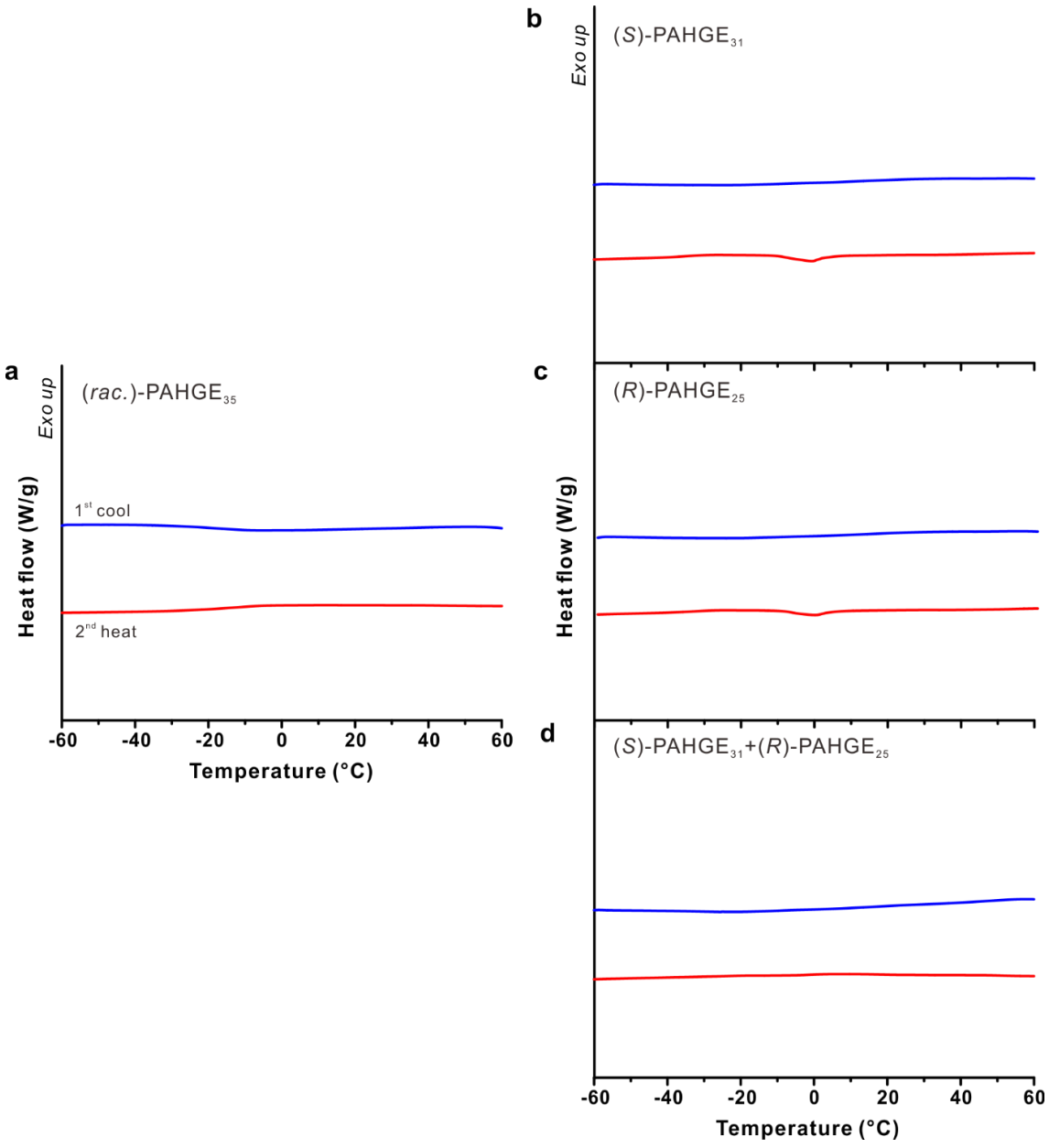

Figure 20. DSC thermograms of (a) (*rac.*)-$PAHGE_{35}$, (b) (*S*)-$PAHGE_{31}$, (c) (*R*)-$PAHGE_{25}$ and (d) 1:1 blend of (*S*)-$PAHGE_{31}$ and (*R*)-$PAHGE_{25}$.

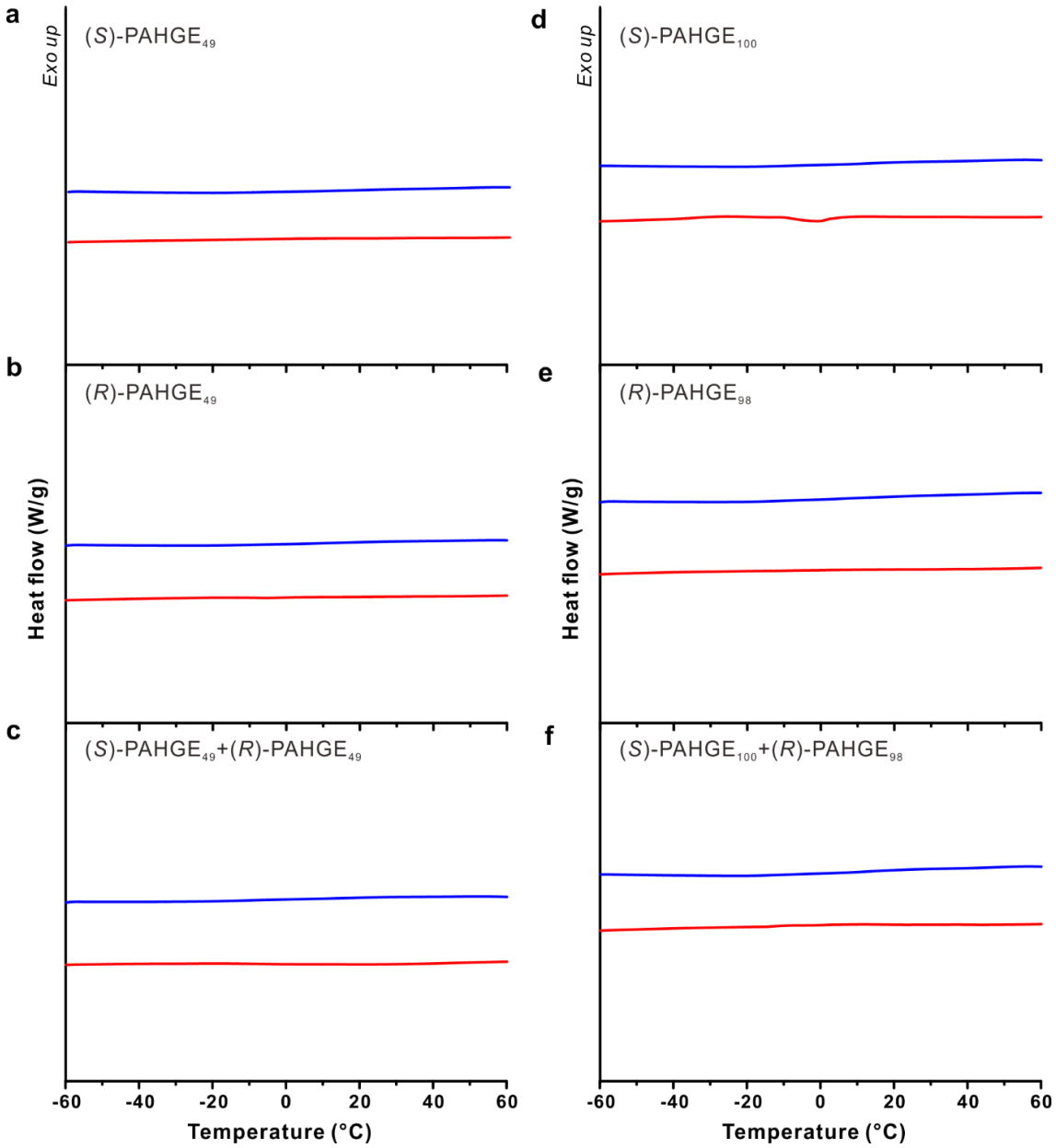

Figure 21. DSC thermograms of (a) (*S*)-PAHGE$_{49}$, (b) (*R*)-PAHGE$_{49}$,(c) 1:1 blend of (*S*)-PAHGE$_{49}$ and (*R*)-PAHGE$_{49}$, (d) (*S*)-PAHGE$_{100}$, (e) (*R*)-PAHGE$_{98}$ and (f) 1:1 blend of (*S*)-PAHGE$_{100}$ and (*R*)-PAHGE$_{98}$.

The HGE monomer was synthesized using an identical procedure as AHGE monomer except for using 1-hexanol instead of 6-azido-1-hexanol (Figure 22 (a)). Atactic and isotactic PHGEs were obtained via *t*-Bu-P_4-catalyzed AROP as well (Figure 22 (b)). As a preliminary study to investigate the effect of azide group on the crystallization of PAHGEs, only three polymers at fixed molecular weight (6,000 g/mol) each from the racemic, (*S*)- and (*R*)-HGE monomers were prepared. The structure of the monomer and corresponding polymer were identified by ^{1}H and ^{13}C NMR spectroscopy (Figure 23 and 24).

From the ^{1}H NMR spectrum, $M_{n.NMR}$ of (*S*)-$PHGE_{37}$ (entry 2 in Table 4) was calculated from integration value of the peaks assigned to polyether backbone (3.70–3.35 ppm, DP × 7H), methylene or methyl groups on each side chain (Figure 24 (a)); $M_{n.NMR}$ = 108.14 (molecular weight of benzyl alcohol) + 158.24 (molecular weight of the HGE monomer) × 37 = 5,963.02 g/mol ≈ 6,000 g/mol. The $M_{n.GPC}$s obtained from GPC measurements in THF using polystyrene (PS) as a standard were always lower than the $M_{n.NMR}$s, but the tendency was consistent (Table 4 and Figure 26). However, PHGEs did not show high isotacticity either (72% in average) similar to the PAHGEs, whereas the (*rac.*)-$PHGE_{40}$ (entry 1) correctly gave a triplet with the ratio between the content of *mm*, *mr*/*rm* and *rr* triad as ratio of 1:2:1 (Figure 25). This implies that the %*ee* values of the chiral HGE monomers would not be high enough.

As revealed by DSC measurement, the effect of azide group on crystallization was striking. (*S*)-$PHGE_{37}$ and (*R*)-$PHGE_{42}$ showed crystallization followed by melting transition behavior (Figure 27 and Table 5). (*rac.*)-$PHGE_{40}$ was still amorphous which reflects the principle that isotacticity or regular arrangement of side chains improve the crystallinity of a given polymer. The T_g value was not determined within the current measurement range of -80 to 70 °C. It is reasonable because the T_g of the isotactic poly(*n*-butyl glycidyl ether) with the %[*mm*] value of 86.4 was -77 °C.[11] The isotacticity of (*S*)-$PHGE_{37}$ was only 5% higher than that of (*R*)-$PHGE_{42}$, but the slight difference not only increased the crystallization temperature (T_c), T_m and related enthalpies (ΔH_c and ΔH_m) but also affected the physical appearance of the polymers. At room temperature, (*S*)-$PHGE_{37}$ was alike self-standing gel and (*R*)-$PHGE_{42}$ was an oil, all of which were more viscous than the atactic counterpart (Figure 28).

Nevertheless, the crystallizable and isotactic PHGEs did not show the stereocomplexation behavior. When polymeric stereocomplex is formed, crystallinity and T_m vastly increases along with a formation of new type of crystallites based on complementary interaction between enantiomeric polymer chains. Here, 1:1 blend of (*S*)- and (*R*)-polymer was also crystallizable but all of the T_c, T_m, ΔH_c and ΔH_m were significantly reduced compared to those of each parent polymer. The reduction of the overall crystallinity or negative contribution to each other may arise because the two kinds of homocrystals acted as an obstacle by limiting space thus preventing further growth of crystals.

In brief, the HGE monomer was synthesized as an analogue of the AHGE monomer without azide

moiety. The atactic and isotactic PHGEs with the similar molecular weight were prepared by the *t*-Bu-P_4-catalyzed AROP, but the polymers were not perfectly isotactic either. The DSC characterization of the PHGEs including the 1:1 blend of two enantiomeric polymers gave three conclusions; 1) Azide group interrupts the chain packing and ability to be crystallized. 2) The more isotactic polymer possesses higher T_c, T_m, ΔH_c and ΔH_m if crystallizable. 3) Neither PAHGEs nor PHGEs showed the stereocomplexation.

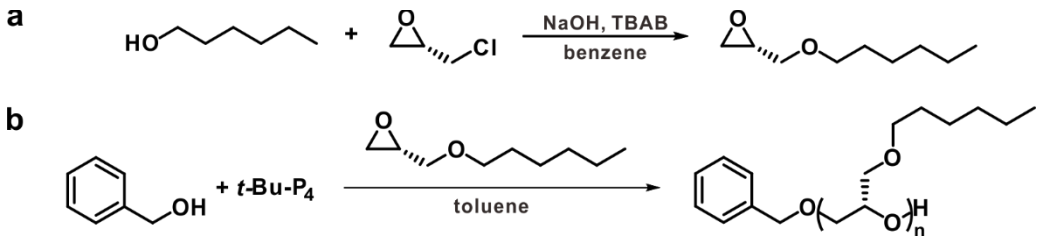

Figure 22. Synthetic scheme of (a) the (*S*)-HGE monomer and (b) the (*S*)-PHGE.

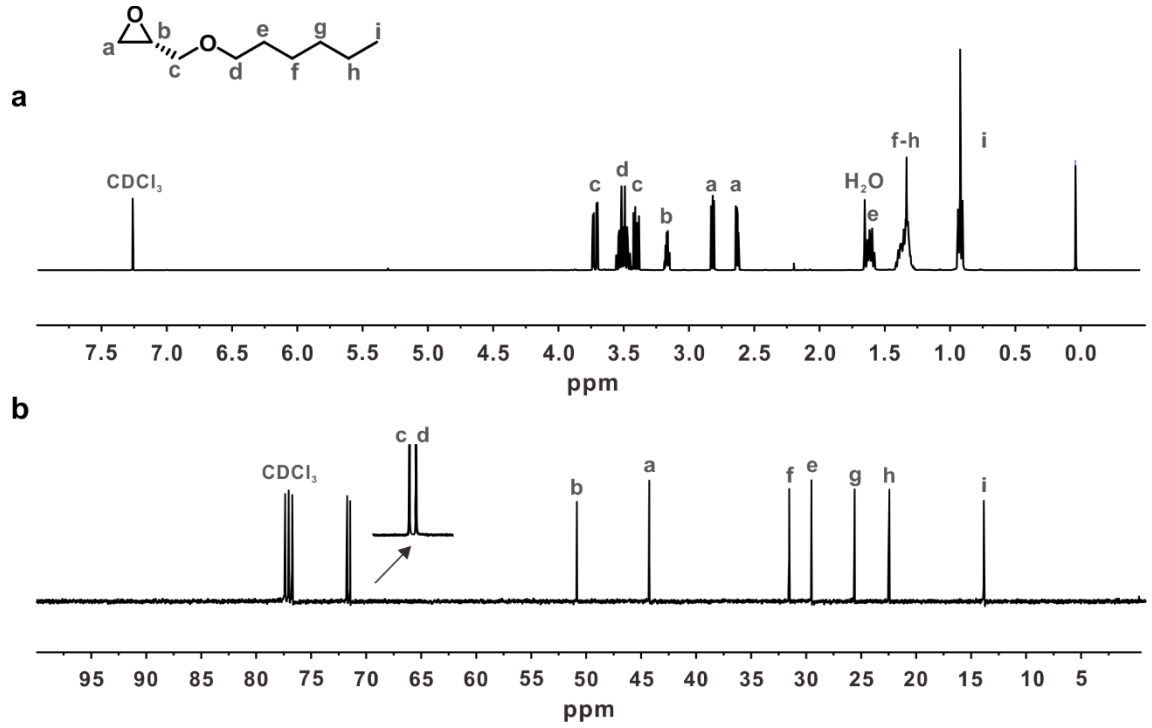

Figure 23. Representative (a) ^{1}H and (b) ^{13}C NMR spectrum of the (*S*)-HGE monomer.

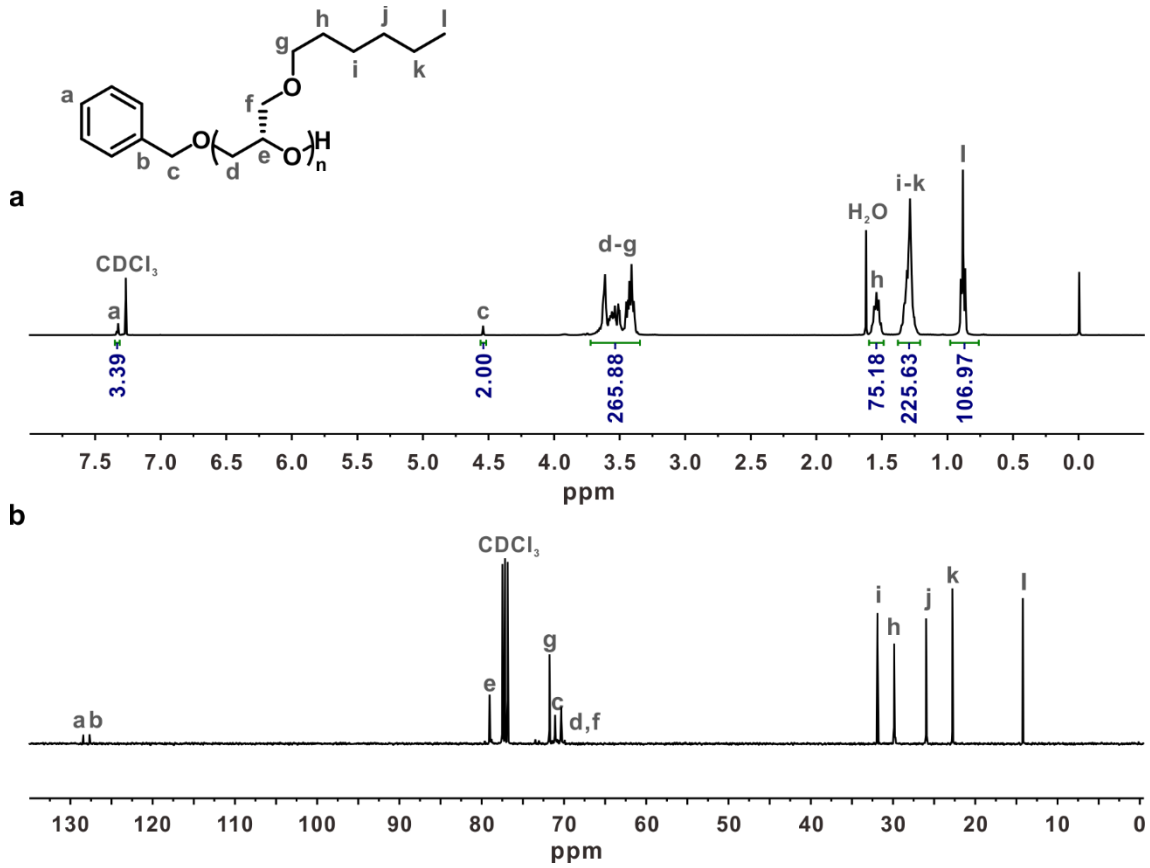

Figure 24. Representative (a) ^{1}H and (b) ^{13}C NMR spectrum of the (*S*)-$PHGE_{37}$ (entry 2 in Table 4).

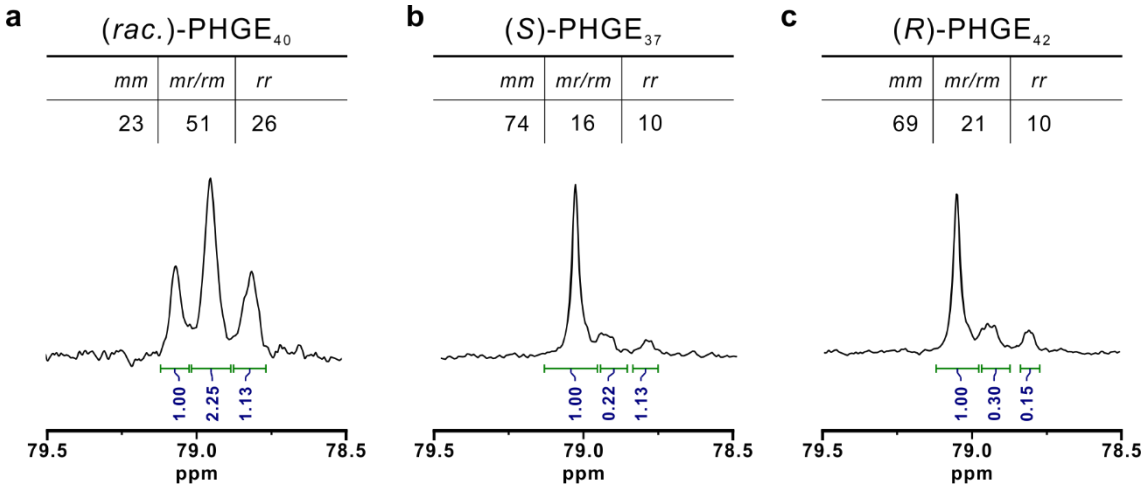

Figure 25. Expanded ^{13}C NMR spectra of PHGEs for tacticity analysis.

Table 4. Characterization data for PHGEs.

Entry		Polymer composition (NMR)	M_n (^{1}H NMR, g/mol)	M_n[a] (GPC, g/mol)	M_w/M_n[a] (GPC)	[mm] [b] (^{13}C NMR, %)
1	(rac.)	$PHGE_{40}$	6,400	5,430	1.06	23
2	(S)	$PHGE_{37}$	6,000	5,000	1.08	74
3	(R)	$PHGE_{42}$	6,800	5,580	1.07	69

[a] Determined by GPC (eluent: THF, calibration: PS). [b] Determined by ^{13}C NMR (from methine peak at 79.0 ppm).

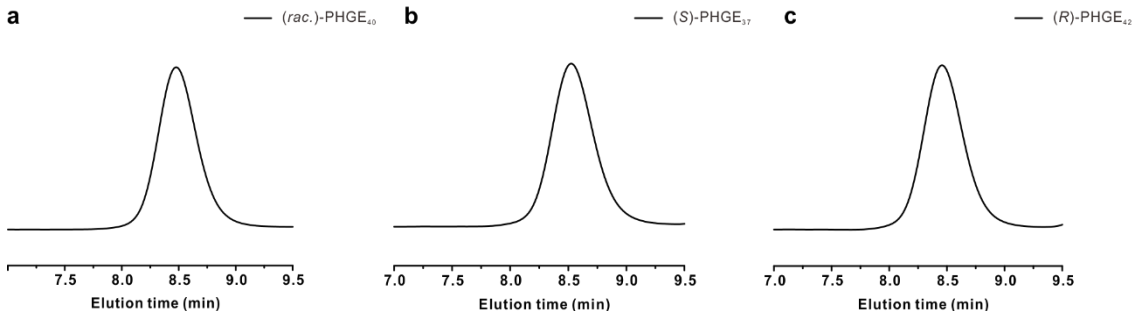

Figure 26. GPC traces of (a) (*rac.*)-$PHGE_{40}$, (b) (*S*)-$PHGE_{37}$ and (c) (*R*)-$PHGE_{42}$ (eluent: THF, calibration: PS).

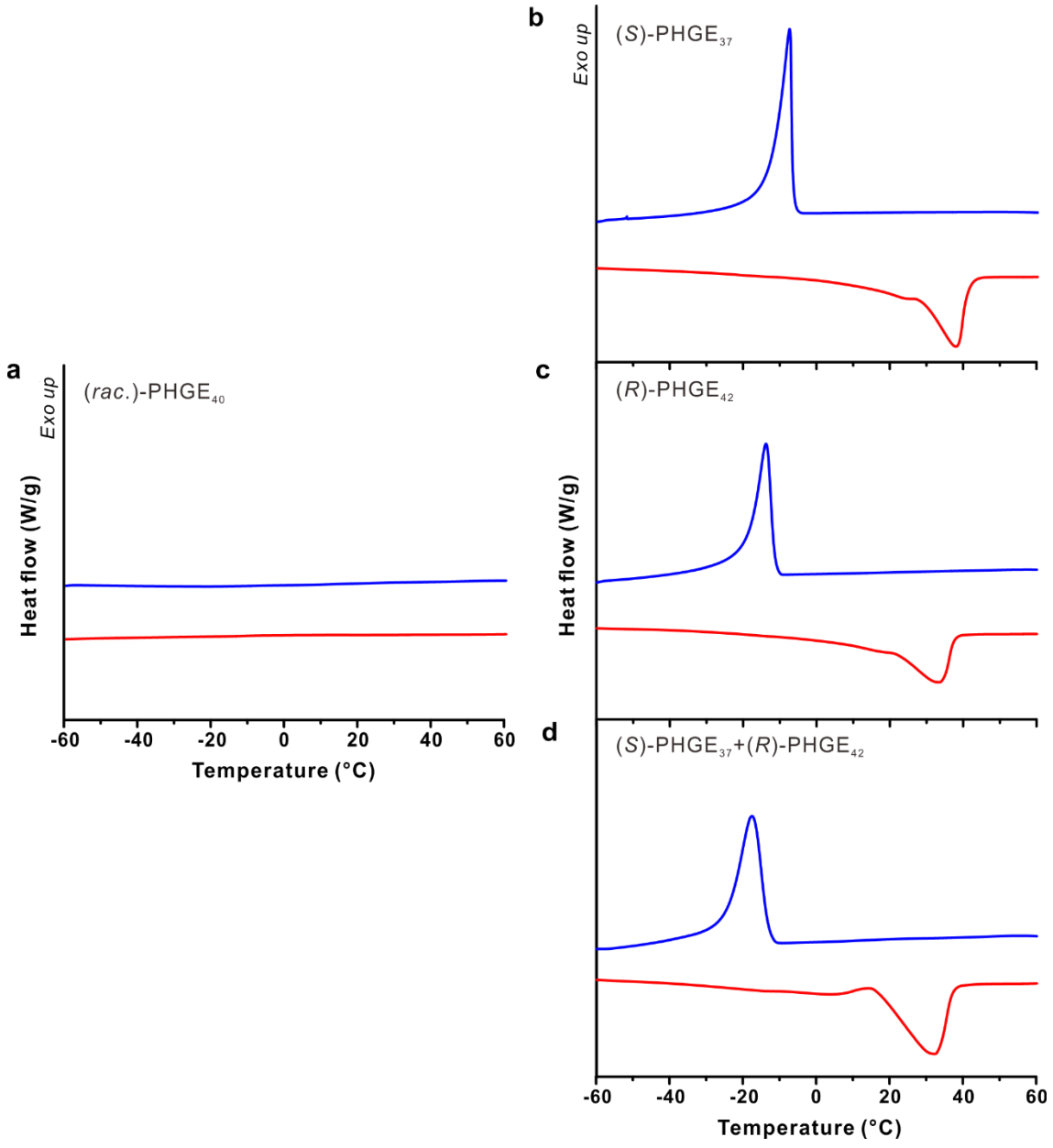

Figure 27. DSC thermograms of (a) (*rac.*)-$PHGE_{40}$, (b) (*S*)-$PHGE_{37}$, (c) (*R*)-$PHGE_{42}$ and (d) 1:1 blend of (*S*)-$PHGE_{37}$ and (*R*)-$PHGE_{42}$.

Table 5. Phase transition behaviors for PHGEs.

	Polymer composition (NMR)	T_c (℃)	ΔH_c (J/g)	T_m (℃)	ΔH_m (J/g)	[mm] [a] (^{13}C NMR, %)
(rac.)	$PHGE_{40}$	-	-	-	-	23
(S)	$PHGE_{37}$	-7.63	59.60	37.71	62.25	74
(R)	$PHGE_{42}$	-13.82	49.27	33.37	52.85	69
	$PHGE_{37}$ +$PHGE_{42}$ (1:1 blend)	-17.47	40.08	3.78 31.93	4.798 30.83	

[a] Determined by ^{13}C NMR (from methine peak at 79.0 ppm).

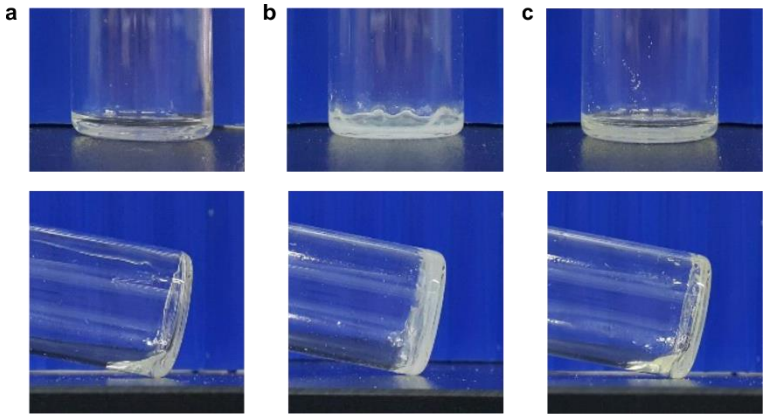

Figure 28. Photographs of (a) (*rac.*)-$PHGE_{40}$, (b) (*S*)-$PHGE_{37}$ and (c) (*R*)-$PHGE_{42}$.

IV. Conclusion

In conclusion, we reported the synthesis of chiral azidohexyl glycidyl ether (AHGE) and hexyl glycidyl ether (HGE) monomer. *t*-Bu-P_4-assisted anionic ring opening polymerization afforded two kinds of isotactic PAHGEs and PHGEs, i.e. (*S*)- and (*R*)-polymers, with various molecular weights. Unfortunately, ^{13}C NMR revealed that all the polymers are not fully isotactic ([*mm*] of 77% for PAHGEs and of 72% for PHGEs in average). The lacking isotacticity is likely due to low enantiopurity of the chiral monomers although the values have not been determined yet. Despite the low isotacticity, the polymers were subjected to GPC and/or DSC analysis to observe how each enantiomeric polymer and their mixture behave or eventually whether stereocomplexation occurs. However, in the case of PAHGEs, two separate GPC measurements gave totally different results and all of them were amorphous regardless of tacticity because of azide groups. Instead, PHGEs, the analogues of PAHGEs without the azide groups, showed the crystallization and melting transition behavior except for the atactic PHGE. However, T_c, T_m, ΔH_c and ΔH_m were decreased in the enantiomeric mixture implying the absence of stereocomplexation in PHGEs.

Although there still remain the issues to achieve perfectly isotactic polymer and appropriately design the monomer to fit the goal of this research, the study on chiral polyethers will provide interesting and unique opportunities in the development of polymer-based therapeutics or biomaterials.

V. References

(1) Wilms, D.; Striba, S.-E.; Frey, H. *Acc. Chem. Res.* **2010**, *43*, 129–141.

(2) Thomas, A.; Müller, S. S.; Frey, H. *Biomacromolecules* **2014**, *15*, 1935–1954.

(3) Veronese, F. M.; Pasut, G. *Drug Discov. Today* **2005**, *10*, 1451–1458.

(4) Liu, G.; Li, Y.; Yang, L.; Wei, Y.; Wang, X.; Wang, Z.; Tao, L. *RSC Adv.* **2017**, *7*, 18252–18259.

(5) Son, S.; Shin, E.; Kim, B.-S. *Macromolecules* **2015**, *48*, 600–609.

(6) Song, J.; Palanikumar, L.; Choi, Y.; Kim, I.; Heo, T. Y.; Ahn, E.; Choi, S. H.; Lee, E.; Shibasaki, Y.; Ryu, J. H.; Kim, B.-S. *Polym. Chem.* **2017**, *8*, 7119–7132.

(7) Lee, J.; McGrath, A. J.; Hawker, C. J.; Kim, B.-S. *ACS Macro Lett.* **2016**, *5*, 1391–1396.

(8) Childers, M. I.; Longo, J. M.; Van Zee, N. J.; Lapointe, A. M.; Coates, G. W. *Chem. Rev.* **2014**, *114*, 8129–8152.

(9) Geyer, R.; Jambeck, J. R.; Law, K. L. *Sci. Adv.* **2017**, *3*, e1700782.

(10) Schilling, F. C.; Tonelli, A. E. *Macromolecules* **1986**, *19*, 1337–1343.

(11) Thomas, R. M.; Widger, P. C. B.; Ahmed, S. M.; Jeske, R. C.; Hirahata, W.; Lobkovsky, E. B.; Coates, G. W. *J. Am. Chem. Soc.* **2010**, *132*, 16520–16525.

(12) Hirahata, W.; Thomas, R. M.; Lobkovsky, E. B.; Coates, G. W. *J. Am. Chem. Soc.* **2008**, *130*, 17658–17659.

(13) McGrath, A. J.; Shi, W.; Rodriguez, C. G.; Kramer, E. J.; Hawker, C. J.; Lynd, N. A. *Polym. Chem.* **2015**, *6*, 1465–1473.

(14) Isono, T.; Asai, S.; Satoh, Y.; Takaoka, T.; Tajima, K.; Kakuchi, T.; Satoh, T. *Macromolecules* **2015**, *48*, 3217–3229.

(15) Eβwein, B.; Molenberg, A.; Möller, M. *Macromol. Symp.* **1996**, *107*, 331–340.

(16) Eβwein, B.; Steidl, N. M.; Möller, M. *Macromol. Rapid Commun.* **1996**, *17*, 143–148.

(17) Misaka, H.; Sakai, R.; Satoh, T.; Kakuchi, T. *Macromolecules* **2011**, *44*, 9099–9107.

(18) Satoh, Y.; Miyachi, K.; Matsuno, H.; Isono, T.; Tajima, K.; Kakuchi, T.; Satoh, T. *Macromolecules* **2016**, *49*, 499–509.

(19) Isono, T.; Miyachi, K.; Satoh, Y.; Sato, S.-I.; Kakuchi, T.; Satoh, T. *Polym. Chem.* **2017**, *8*, 5698–5707.

(20) Isono, T.; Lee, H.; Miyachi, K.; Satoh, Y.; Kakuchi, T.; Ree, M.; Satoh, T. *Macromolecules* **2018**, *51*, 2939–2950.

(21) Slager, J.; Domb, A. J. *Adv. Drug Deliv. Rev.* **2003**, *55*, 549–583.

(22) Fox, T. G.; Garrett, B. S.; Goode, W. E.; Gratch, S.; Kincaid, J. F.; Spell, A.; Stroupe, J. D. *J. Am. Chem. Soc.* **1958**, *80*, 1768–1769.

(23) Liquori, A. M.; Anzuino, G.; Coiro, V. M.; D'Alagni, M.; De Santis, P.; Savino, M. *Nature* **1965**, *206*, 358–362.

(24) Mitsui, Y.; Iitaka, Y.; Tsuboi, M. *J. Mol. Biol.* **1967**, *24*, 15–28.

(25) Ikada, Y.; Jamshidi, K.; Tsuji, H.; Hyon, S.-H. *Macromolecules* **1987**, *20*, 904–906.

(26) Kumaki, J.; Kawauchi, T.; Okoshi, K.; Kusanagi, H.; Yashima, E. *Angew. Chem. Int. Ed.* **2007**, *119*, 5444–5447.

(27) Ren, J. M.; Lawrence, J.; Knight, A. S.; Abdilla, A.; Zerdan, R. B.; Levi, A. E.; Oschmann, B.; Gutekunst, W. R.; Lee, S.-H.; Li, Y.; McGrath, A. J.; Bates, C. M.; Qiao, G. G.; Hawker, C. J. *J. Am. Chem. Soc.* **2018**, *140*, 1945–1951.

(28) Serizawa, T.; Hamada, K.; Akashi, M. *Nature* **2004**, *429*, 52–55.

(29) Li, Y.; Fukushima, K.; Coady, D. J.; Engler, A. C.; Liu, S.; Huang, Y.; Cho, J. S.; Guo, Y.; Miller, L. S.; Tan, J. P. K.; Ee, P. L. R.; Fan, W.; Yang, Y. Y.; Hedrick, J. L. *Angew. Chem. Int. Ed.* **2013**, *125*, 702–706.

(30) Tsuji, H. *Macromol. Biosci.* **2005**, *5*, 569–597.

(31) Li, Z.; Tan, B. H.; Lin, T.; He, C. *Prog. Polym. Sci.* **2016**, *62*, 22–72.

(32) Longo, J. M.; DiCiccio, A. M.; Coates, G. W. *J. Am. Chem. Soc.* **2014**, *136*, 15897–15900.

(33) Zhu, J.-B.; Watson, E. M.; Tang, J.; Chen, E. Y.-X. *Science* **2018**, *360*, 398–403.

(34) Longo, J. M.; Sanford, M. J.; Coates, G. W. *Chem. Rev.* **2016**, *116*, 15167–15197.

(35) Colclough, M. E.; Desai, H.; Millar, R. W.; Paul, N. C.; Stewart, M. J.; Golding, P. *Polym. Adv. Technol.* **1994**, *5*, 554–560.

(36) Gaur, B.; Lochab, B.; Choudhary, V.; Varma, I. K. *J. Macromol. Sci., Polym. Rev.* **2003**, *43*, 505–545.

(37) Brochu, S.; Ampleman, G. *Macromolecules* **1996**, *29*, 5539–5545.

Acknowledgments

This work was supported by the National Research Foundation of Korea (NRF) grant funded by the Korea government (MSIT) (No.2018R1A5A1025208). The author thanks J. Lee for providing (*rac.*)-PAHGE$_{35}$ and T. Kim for the FT-IR measurement. The author acknowledges Prof. B.-S. Kim, Prof. T.-H. Kwon, Prof. D. W. Lee, Prof. Young. S. Park and Prof. T. Isono for the thoughtful discussion as well.